FULL PAPER

Photoredox/Cobalt Dual Catalyzed Decarboxylative Elimination of Carboxylic Acids: Development and Mechanistic Insight

Kaitie C. Cartwright[a], Ebbin Joseph[a], Chelsea G. Comadoll[a], and Jon A. Tunge[a]*

Abstract: Recently, dual catalytic strategies towards the decarboxylative elimination of carboxylic acids have gained attention. Our lab previously reported a photoredox/cobaloxime dual catalytic method that allows the synthesis of enamides and enecarbamates directly from *N*-acyl amino acids that avoids the use of any stoichiometric reagents. Further development, detailed herein, has improved upon this transformation's utility and further experimentation has provided new insights into the reaction mechanism. These new developments and insights are anticipated to aid in the expansion of photoredox/cobalt dual catalytic systems.

1. Introduction

The pairing of a photoredox catalyst with a cooperative transition metal catalyst has become a powerful design strategy for photo-induced decarboxylative transformations.[1] These dual catalytic methods allow for direct functionalization of readily available feedstock carboxylic acids and often benefit from improved chemoselectivity, economy, and broader scope. Decarboxylative elimination is one such transformation that has recently been explored using the photoredox/transition metal dual catalytic strategy. These eliminations furnish olefins, arguably one of the most versatile functional groups, from feedstock carboxylic acids (Scheme 1).[2,3] Building upon the pioneering work of Kochi, these recent reports represent more efficient and practical variants of Kochi's initial decarboxylative elimination methodology,[4] and also offer an alternative to recent related methods involving stoichiometric oxidants.[5] One strategy used by Glorius[3a] makes use of redox-active esters[6] to achieve a reductive radical decarboxylation and generate olefins through the action of a copper co-catalyst (Scheme 1A). The downside of this approach is the need to pre-activate the carboxylic acid as an active ester, which detracts from the economy of the method.[7] Another approach, simultaneously developed by the Ritter group and our lab, involves the direct decarboxylation of the carboxylic acids followed by subsequent elimination through the combination of decarboxylation and hydrogen evolution (Scheme 1B & 1C).[3b,c] Shortly thereafter, Larionov reported a decarboxylative elimination of biomass-derived feedstocks utilizing various acridine/cobaloxime dual catalytic systems (Scheme 1D).[3d] In addition, Liu/Wu report a similar decarboxylative elimination process in a Heck-type coupling (Scheme 1E).[3e] These direct approaches make use of a photoredox catalyst to achieve oxidative decarboxylation in tandem with a cobaloxime catalyst to perform the needed hydrogen atom transfer (HAT) (Scheme 1B-E).[8]

A. Glorius Redox-Active Ester-Promoted Olefination

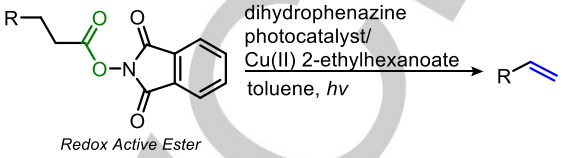

B. Ritter Ir^{+}/Co Dehydrogenative Decarboxyolefination

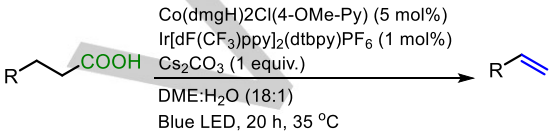

C. Tunge Acr^{+}/Co Decarboxylative Elimination

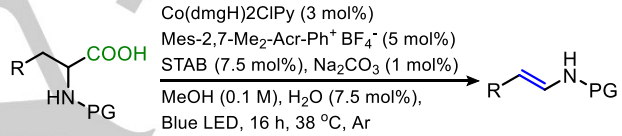

D. Larionov Dehydrodecarboxylation of Biomass

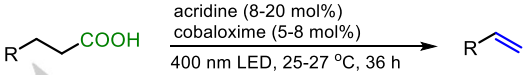

E. Liu & Wu Acr^{+}/Co Decarboxylative Heck-like Coupling

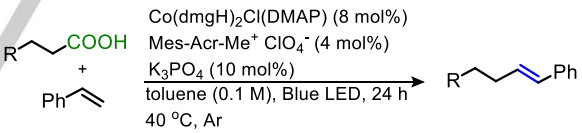

Scheme 1: Dual catalytic decarboxylative olefination methods

These new methods that merge decarboxylation with hydrogen evolution chemistry have provided new routes for decarboxylative elimination that proceed under mild conditions and do not require the use of stoichiometric additives, namely, a stoichiometric oxidant.[8a] Despite this surge of reports, there are currently gaps in our understanding of how these transformations occur and the factors that influence their success. To aid in bridging this gap, our decarboxylative elimination process was further explored to understand the mechanism and influences of catalyst variations on reactivity, improve upon utility, as well as assess the advantages and limitations of this methodology. In addition, comparisons to the related methods recently reported are drawn. We anticipate that further development and understanding of this transformation can aid in the synthetic application of these methods and the development of transformations that operate under similar dual catalytic conditions.

[a] Department of Chemistry, The University of Kansas, 1567 Irving Hill Rd., Lawrence, KS, 66045
E-mail: tunge@ku.edu

Supporting information for this article is given via a link at the end of the document.

2. Results and Discussion

2.1.1 Acridinium/Cobalt Catalyst Optimization

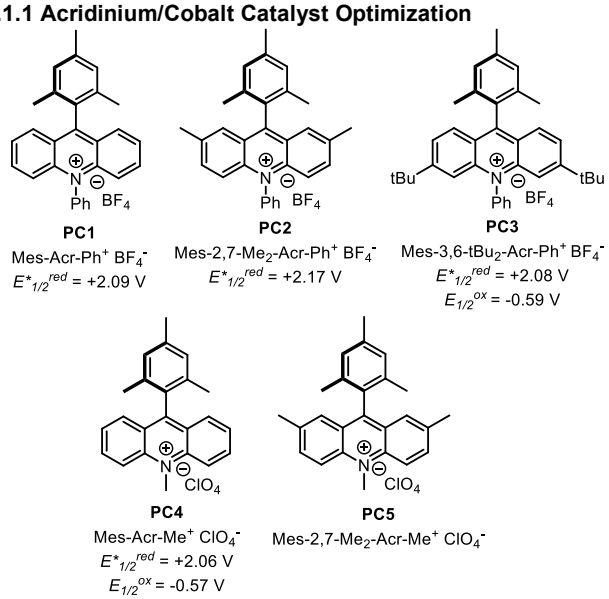

Figure 1: Acridinium photocatalysts

Further exploration of our decarboxylative elimination began with a return to screening different photocatalysts and cobaloxime catalysts under our previously established conditions.[3c] First, additional acridinium photocatalysts were investigated (Table 1, entries 1-5). Theoretically, all of the acridinium photocatalysts should be sufficiently oxidizing to generate a carboxyl radical from a carboxylate.[9] Despite this, significant yield variations were observed for the decarboxylative elimination of amino acids when changes were made to the acridinium catalyst.

Table 1: Catalyst screening

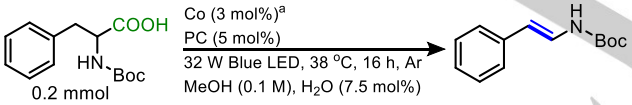

Entry	Cobalt Catalyst	Photocatalyst	Yield	Isomer Ratio (E:Z)[b]
1	$Co(dmgH)_2ClPy$	PC2	82%	65:35
2	$Co(dmgH)_2ClPy$	PC1	15%	69:31
3	$Co(dmgH)_2ClPy$	PC3	56%	73:27
4	$Co(dmgH)_2ClPy$	PC4	69%	65:35
5	$Co(dmgH)_2ClPy$	PC5	93%	71:29
6	$Co(dmgH)_2BrPy$	PC2	74%	56:44
7	$Co(dmgBF_2)_2(CH_3CN)_2$	PC2	39%	65:35
8	$Co(dmgH)(dmgH_2)Cl_2$	PC2	63%	67:31
9	$Co(dmgH)(dmgH_2)Br_2$	PC2	59%	64:36
10	B12 [c]	PC2	7%	75:25
11	$Co(salen)_2$ [c]	PC5	27%	74:26
12	$Co(salen)_2$ [d]	PC5	21%	88:12

[a] Cobalt catalysts were subjected to sodium triacetoxyborohydride (STAB) (7.5 mol%) and Na_2CO_3 (1 mol%) in MeOH (see experimental section Pre-Reduction Procedure). [b] Yields reported represent isolated yields and isomer ratios were determined by ^1H NMR. [c] Cobalt was reduced with Zn (3 mol%) in presence of NaCl (10 mol%) in MeOH (see experimental section for further details). [d] No pre-reduction employed.

These studies revealed that the less oxidizing and more reducing catalyst, Mes-2,7-Me_2-Acr-Me^+ ClO_4^- (**PC5**), provided similar or higher yields as compared to the Mes-2,7-Me_2-Acr-Ph^+ BF_4^- (**PC2**) catalyst with amino acid substrates (Figure 1 & Table S1). When applied to other classes of carboxylic acids, the **PC5** catalyst is far superior. Due to the greater generality achieved with **PC5**, it was utilized in all further evaluation of the decarboxylative elimination.

Following the revelation that the acridinium perchlorate **PC5** was superior, the focus turned to exploring changes in the cobaloxime catalyst.[9f] Early studies evaluated the effects of changes in the halogen, Co oxidation state, and the ligand in the cobaloxime and cobalamin catalysts (Table 1, entries 6-12). However, it was quickly realized that the catalyst initially utilized, $Co(dmgH)_2ClPy$ (dmgH = dimethylglyoxime), was the optimal catalyst of this set. Despite this, several enlightening observations were made. First, cobaloximes gave higher yields and conversions compared with the corrin and salen complexes (Table 1, entries 10-12). Of the cobaloximes, complexes with proton bridges in the oxime scaffold outperform the BF_2-bridged species (Table 1, entry 7). The superior results of the proton-bridged cobaloximes compared to the other complexes screened could be a result of the difference in pre-catalyst oxidation state [Co(III) vs. Co(II)]. Lastly, having pyridine as one of the axial ligands produced higher yields as compared to having halides in both axial positions (Table 1, entries 8-9). In addition, having the chlorine ligand instead of bromine influenced the final elimination product yield, with the chloride complex producing the best results (Table 1, entries 1 & 6).

2.1.2 Cobaloxime Ligand Evaluation

To further explore the cobaloxime catalyst in the elimination, other cobaloxime complexes containing a proton-bridged glyoxime equatorial ligand system along with chlorine and nitrogen-base axial ligands were synthesized (Figure 2). Three different oxime ligands were utilized to assess the influence of *cis*-steric demands around the metal center on the elimination.[10]

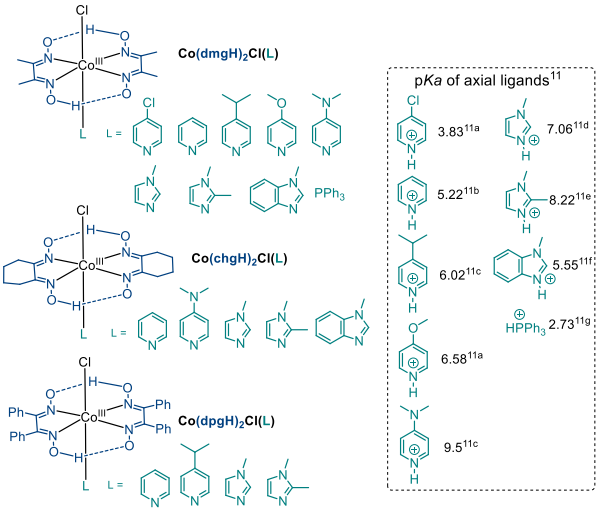

Figure 2: Cobaloxime catalysts investigated

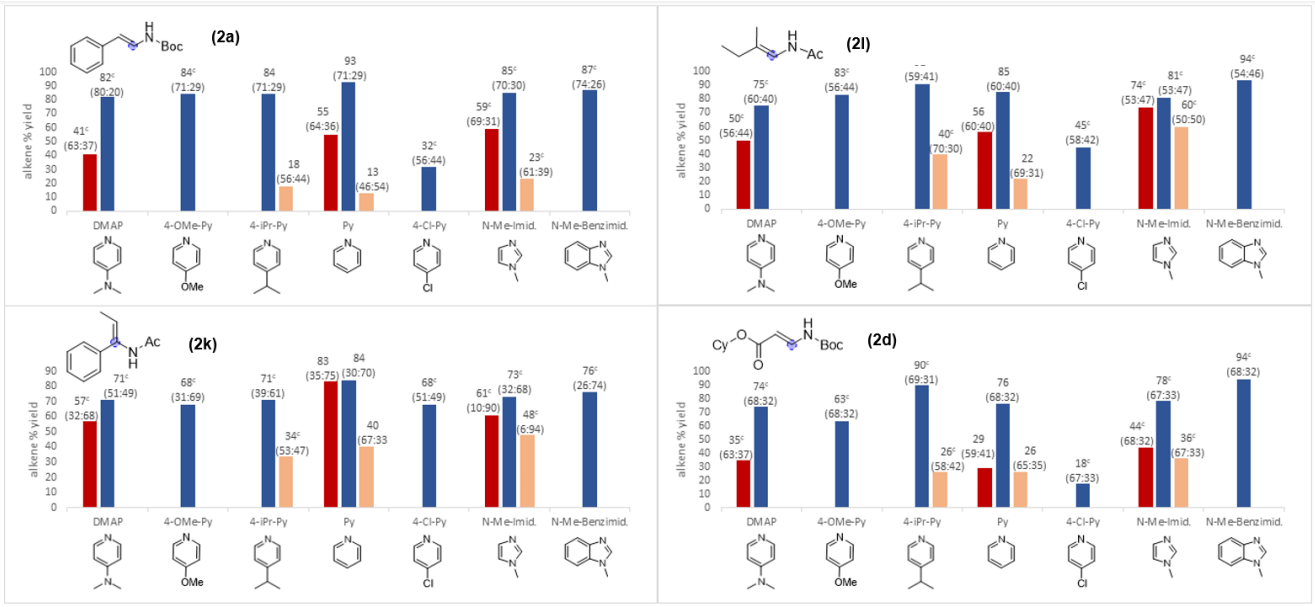

Figure 3: Cobaloxime catalyst screening in enamide and enecarbamate synthesis
[a] Reactions performed with protected amino acids (0.2 mmol), Mes-2,7-Me_2-Acr-Me^+ ClO_4^- (**PC5**, 5 mol%), cobaloxime (3 mol%), STAB (7.5 mol%), and Na_2CO_3 (1 mol%) using the pre-reduction procedure (see Experimental Section for details). [b] Isolated yields are shown. [c] Determined by q^1H NMR vs. pyridine internal standard. [d] *E:Z* isomer ratios shown in parentheses. [e] All catalysts screened provided elimination product, absent bars indicate that the corresponding catalyst was not evaluated. [f] Colored bars correspond to equatorial ligand changes; chgH = red, dmgH = blue, dpgH = yellow.

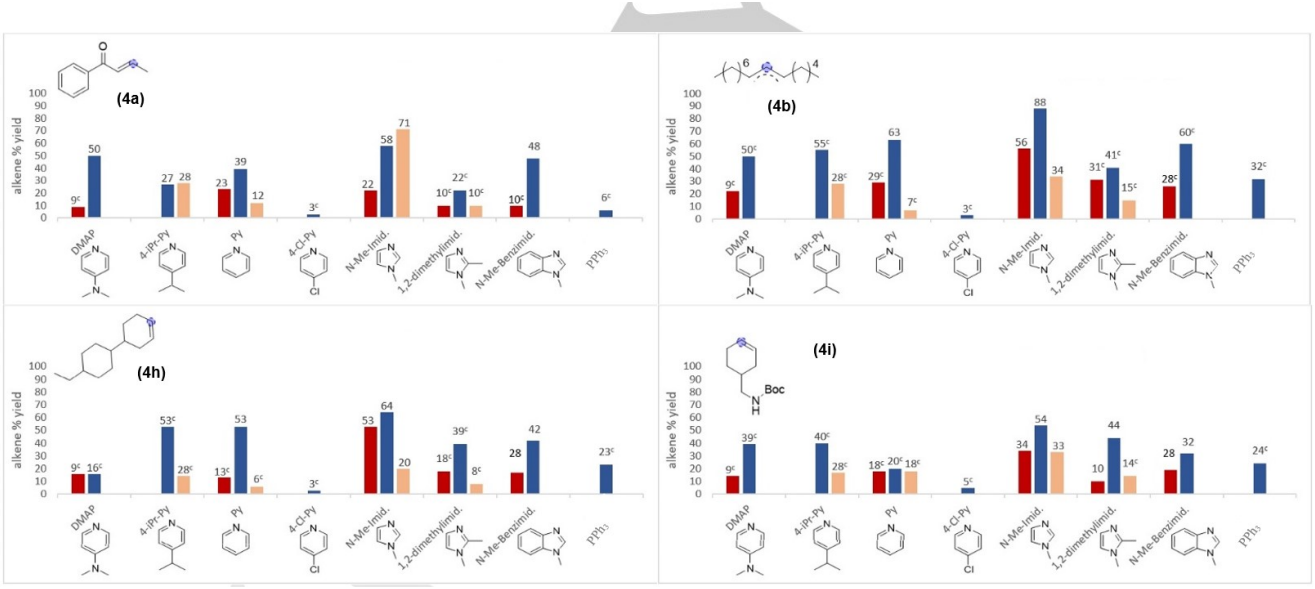

Figure 4: Cobaloxime catalyst screening in alkene formation from α,α-disubstituted carboxylic acids
[a] Reactions performed with protected amino acids (0.2 mmol), Mes-2,7-Me_2-Acr-Me^+ ClO_4^- (**PC5**, 5 mol%), cobaloxime (3 mol%), STAB (7.5 mol%), and Na_2CO_3 (1 mol%) using the pre-reduction procedure (see Experimental Section for details). [b] Isolated yields are shown. [c] Determined by q^1H NMR vs. pyridine internal standard. [d] All ctalyst screened provided elimination product, absent bars indicate that the corresponding catalyst was not evaluated. [e] Colored bars correspond to equatorial ligand changes; chgH = red, dmgH = blue, dpgH = yellow.

For the axial ligands, derivatives of pyridine and imidazole of varying basicity were utilized, as well as triphenylphosphine.[11] These changes were anticipated to influence the stability of the cobalt catalyst and its intermediates, the reduction potentials, the lifetime and reactivity of a cobalt hydride species, the sterics surrounding the metal center, and the rate of hydrogen evolution.[12] Through an evaluation of these ligand effects on our elimination reaction, we hoped to gain better insight into the reaction mechanism.

The cobaloximes synthesized (Figure 2) were first utilized in reactions with four different *N*-protected amino acids (Figure 3). Of the catalysts screened, the dimethylglyoxime (dmgH) ligand provided superior yields in all cases. Apart from 4-chloropyridine, all axial base ligands paired with dmgH provided good yields. Notably, this observation stands in stark contrast to the Ritter methodology, where far superior yields are reported when 4-methoxypyridine is the axial base ligand.[3b] Among this set of reactions, the *E*/*Z* ratios were quite variable. With most axial bases and with all substrates, it appears that the chgH (cyclohexylglyoxime) and dpgH (diphenylglyoxime) catalysts provided greater *Z*-selectivity than the dmgH catalysts; however, these reactions were typically much lower yielding. Despite this, it is interesting to note that the chgH and dpgH catalysts performed better with the more sterically demanding substrates **1k** and **1l** compared to amino acids **1a** and **1d**.

Next, focus was given to evaluating the performance of other α,α-disubstituted carboxylic acids under the decarboxylative elimination conditions since this class of acids has not been systematically investigated by others. Initially, four carboxylic acids were subjected to the elimination reaction conditions using the set of cobaloxime catalysts synthesized (Figure 4). Compared to the amino acids, the changes in cobaloxime had much greater influences on the success of the elimination with the α,α-disubstituted carboxylic acids. In most cases, the dmgH equatorial ligand provided superior yields. Of the axial pyridine ligands screened, pyridine and the more electron-rich 4-*i*Pr-pyridine and DMAP resulted in much better yields than the 4-chloropyridine. However, among the more electron-rich pyridines, no significant trend was observed, as they all provided similar yields of alkene product. Interestingly, in all cases the best yields were obtained with *N*-Me-imidazole as the axial base ligand. Changing to the more electron-rich and sterically more demanding 1,2-dimethylimidazole led to decreased productivity, while the more electron-deficient *N*-Me-benzimidazole provided similar yields to that seen with the pyridine ligands. While it is tempting to attribute the decreased yields with 1,2-dimethylimidazole relative to *N*-Me-imidazole to a steric effect, the benzimidazole ligand provides high yields even with sterically demanding amino acid substrates (Figure 3), indicating that the electronic factors may be more important than sterics. When triphenylphosphine was utilized as the axial ligand, the yields obtained were greatly diminished compared to those seen with *N*-Me-imidazole.

These trends are in line with those outlined by Artero and Coutsolelos in their studies of cobaloximes in photochemical hydrogen production from water.[12a] They found that the *N*-Me-imidazole catalyst had superior stability to the pyridine catalysts employed, providing the highest TON in addition to the highest TOF of their axial ligand set. Thus, the trend in catalyst success observed does appear to be positively correlated to catalyst stability and rate of H_2 generation. When considering the amino acid substrates, the axial ligand may not have a profound influence as a result of the lower pK_a of these carboxylic acids which leads to facile hydrogen evolution (HE). However, carboxylic acids with higher pK_a values experience a greater influence on HE with a change in the catalyst system. Thus, utilizing a cobaloxime catalyst that has been shown to have higher TON and TOF[12a] proved to be most successful with the carboxylic acid substrates that have higher pK_as.

2.1.3 Catalyst Influence on Reaction Rate

To gain more insight into the ligand influences in our system, an evaluation of initial reaction rates was undertaken (Figure 5). First, it is important to note that the reaction was found to be 0th order (Figures S3 and S4) in acid substrate. Such kinetic behavior is usually indicative of a rate-determining photochemical process.[13] Unexpectedly, when evaluating the initial rate difference between amino acid **1a** and **3b**, it was evident that the nature of the carboxylic acid influences the reaction rate, with the α-amino acid **1a** reacting faster than the unfunctionalized acid **3b** (Figure 5A). This was puzzling since the identity of the carboxylic acid is not expected to influence the rate of a 0th-order process. This led us to propose that these acids associate with the photocatalyst differently, influencing photochemical excitation. Indeed, subjecting the acridinium photocatalyst to carboxylate salts like that of **3b** revealed a color change from yellow to red in addition to marked chemical shift changes in ^{1}H NMR of the acridinium catalyst (Figures S5 and S6). Thus, it is possible that the carboxylates serve as counterions to the acridinium. In such a case, the photophysics of the catalyst would be tied to an association event with the cationic acridinium which would be influenced by carboxylate structure.[9f,14]

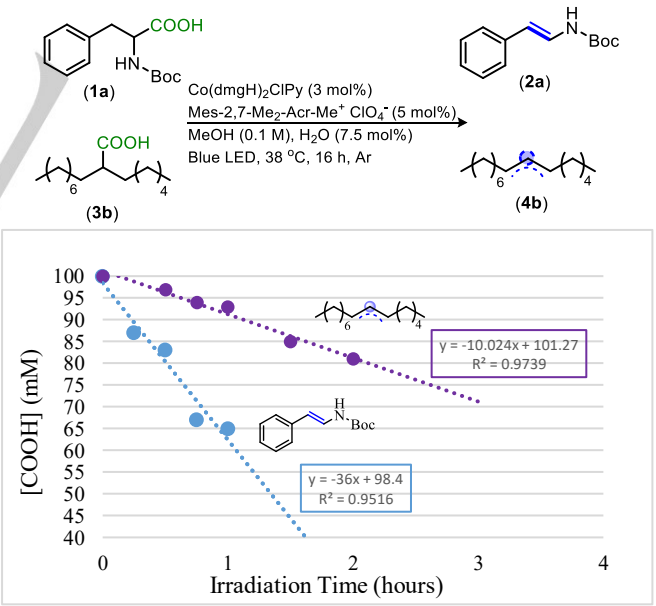

Figure 5: Initial rate influences

[a] Pre-reduction procedure utilized (see Experimental Section for details). [b] Blue line = **1a** to **2a**; purple line = **3b** to **4b**. [c] Data points represent an average of two reactions.

2.2 Substrate Structure and Functional Group Influences

2.2.1 Substrate Scope and Influence

In the first-generation decarboxylative elimination of *N*-acyl amino acids, it was found that the reaction generally produced higher yields when the nitrogen was protected with acyl groups as opposed to carbamate groups;[3c] the only examples where this difference is not significant is with phenylalanine and its derivatives (Table S1, **2a-i**). Several experiments were completed to elucidate the factors that account for these differences.

The potential influence of substrate electronics on the reaction efficiency was determined through pairwise comparison of competitive rates of reaction of *N*-Boc-phenylalanine (**1a**) with its *para*-substituted derivatives (Table S1, **1b-i**). The initial ratios of rates of these reactions were plotted against σ-values in a Hammett plot (Figure S7). The near-zero ρ (-0.05) indicates that the electronic changes in the aromatic side chain are not influencing the relative rates of elimination. In addition, the rate influences of various side chains and *N*-protecting groups were investigated but none of these changes were found to be rate-influencing (Figure S8).

The scope of the carboxylic acids was further explored with CoCl(*N*-Me-imidazole) cobaloximes containing chgH, dmgH, and dpgH ligands (Table 2). Unsubstituted and quaternary acids did not perform well under the standard conditions (low conversions, yields <20%). But, α,α-disubstituted carboxylic acids proved to eliminate successfully. Among these, the architecture of the substrates evaluated had profound influences on the efficiency and regioselectivity of the elimination. Acyclic acids underwent elimination most efficiently when there was less steric hindrance around the carboxylic acid appendage. The more sterically encumbered reactive sites resulted in lower conversions and lower alkene yields (Table 2, **4b-g**). Conversely, cyclic acids benefited from more steric hindrance around the reactive site with greater conversion and alkene yield resulting from these cases compared to the less sterically hindered substrates (Table 2, **4h-p**). In all cases, the elimination was selective for the Hofmann product and the less sterically encumbered olefin, with greater selectivity resulting from increased steric differentiation.

2.2.2 Functional Group Compatibility

An additive robustness screening was completed with **3b** serving as the model substrate (Figure 6).[15] The functionalities in question have been grouped based on the yield of eliminated product (**4b**) obtained in the presence of each additive (Figure 6). Apart from the α,β-unsaturated ketone (**A11**) and aldehyde (**A12**), all of the reactions proceeded without side product formation. The olefin in ketone **A11** was reduced to provide 14% yield of the saturated ketone product and the remaining **A11** was recovered. Conversely, the aldehyde **A12** produced a complex mixture of side products. The additives that caused moderate to low yields of olefin were speculated to interrupt the catalytic cycle, as these reactions resulted in low conversion.

Although the reaction proved to be tolerant of a variety of functionalities, several revealing observations were made through the course of this screening. For one, when terminal olefin **A1** was employed in the reaction, no isomerization of the olefin was observed. This was surprising as the Co(III) hydride is proposed

Table 2: α,α-disubstituted carboxylic acids scope

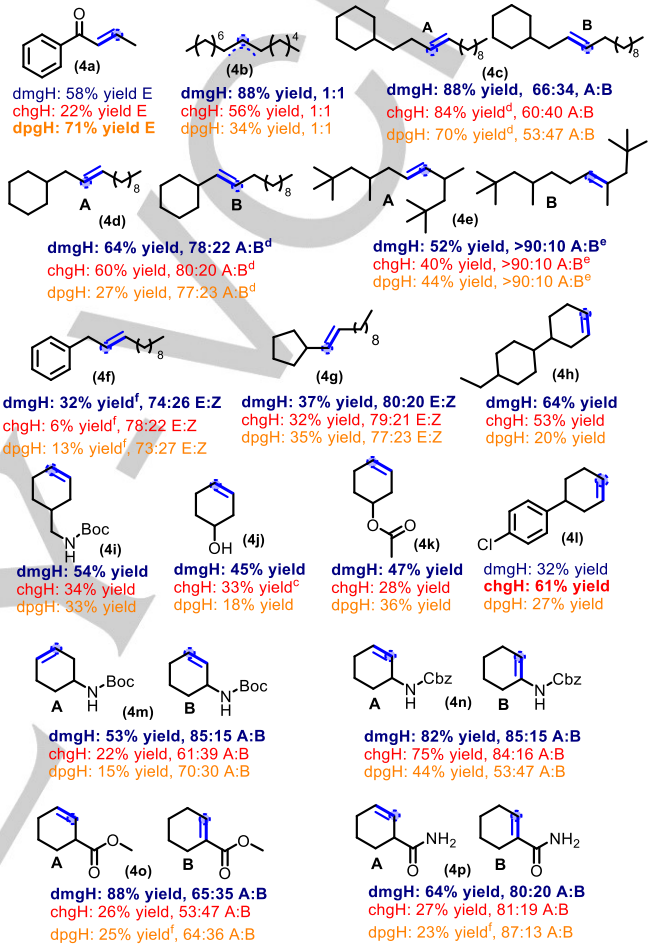

[a] Reaction performed at 0.2 mmol using pre-reduction method (see Experimental Section) and isolated yields are reported unless otherwise denoted. [b] Regioisomer ratios were determined using ^{1}H & COSY NMR. [c] Yields determined with q^{1}H NMR. [d] Isolated >95:5 E/Z ratio. [e] Mix of E/Z isomers for each regioisomer. [f] Isolated >95:5 regioisomer ratio; isolated with alkane product and yield adjusted accordingly. [g] Geometric isomers were determined with NOESY.

to perform isomerizations of terminal olefins to the more thermo-stable internal olefins.[16] This reaction also performed well in the presence of the potential radical trap **A2**, with no formation of the coupled species.[17] Moderately Lewis-basic additives such as **A14-16** and **A20-21** led to lower alkene formation. It is likely that these additives inhibit the catalytic cycle via undesired coordination with the cobalt catalyst, making a less active catalyst. Notably, excess addition of a good ligand for catalysis does not affect the reaction efficiency (**A6**). In addition to deactivating bases, the reaction performs poorly in the presence of allylic chlorides **A22** and **A23**. Most intriguing is the reactivity

interruption that resulted from the use of unsubstituted (**A17-18**) or quaternary (**A19**) carboxylic acids in the reaction. Both **A17** and **A19** resulted in ~10% yield of desired alkene **4b**. Further analysis showed that **A17** and **A19** did not undergo any elimination when used as additives. The reaction with **A18** lead to product **4b** in 36% yield and the reduced alkane side product in 16% yield, leaving **A18** completely intact. These results seem to suggest that the unsubstituted and quaternary acids interrupt the catalytic cycle.[18] This stands in stark contrast to the reports by Ritter,[3b] Larionov,[3d] and Liu/Wu;[3e] much of their substrate scope and highest yields were derived from unsubstituted carboxylic acids.

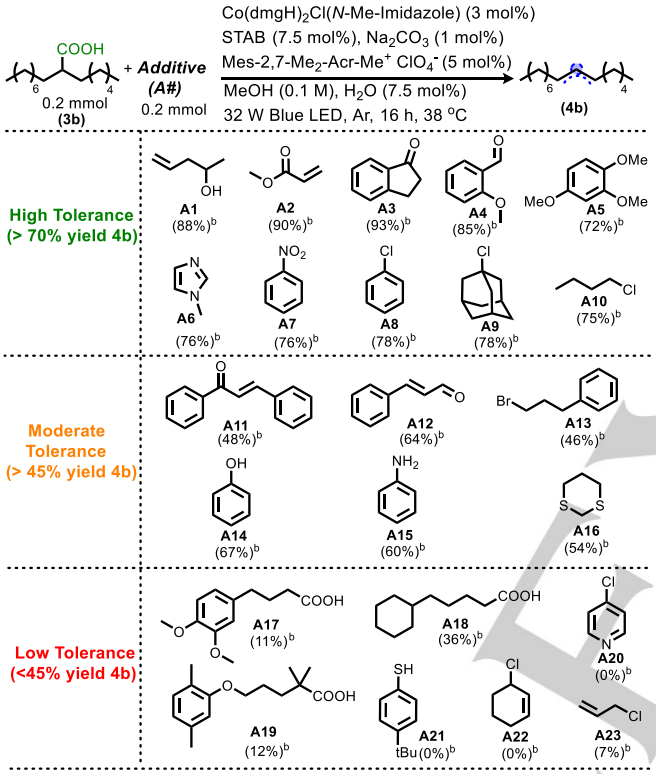

Figure 6: Additive robustness screening

[a] Reactions performed with **2a** (0.2 mmol) and respective additive (0.2 mmol) with Co(dmgH)$_2$Cl(*N*-Me-Imidazole) (3 mol%), STAB (7.5 mol%), Na_2CO_3 (1 mol%), **PC5** (5 mol%), H_2O (7.5 mol%), MeOH (2 mL) and irradiated for 16 h (*in situ* reduction procedure, see Experimental Section). [b] () yields are Isolated yields of **4b**.

2.3 Effects of Reaction Conditions and Additives

In addition to the further evaluation of the catalyst system used, the effect of catalytic additives was also further investigated. Previously, we identified that a pre-reduction process employing sodium triacetoxyborohydride (STAB) and a catalytic amount of base provided a pre-catalyst that produced the highest yields. A 3:5 ratio of cobaloxime to acridinium proved optimal, and inclusion of a catalytic amount of water in the reaction mixture improved overall yields (Scheme 2).

In our re-evaluation of these conditions, the influence of the pre-reduction and the additives on the success of the elimination was

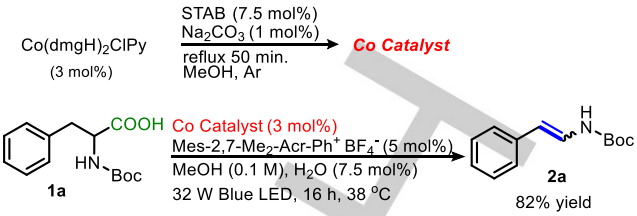

Scheme 2: Decarboxylative elimination of *N*-acyl amino acids[3c]

judged using amino acid **1a** and carboxylic acid **3b** as the model substrates (Table 3). Diminished yields were observed when water concentration was increased above 11 mol % in the original methodology for enamide synthesis. This was suspected to be due to competing hydrolysis that would degrade the desired enamide and enecarbamate products. Thus, we expected that the competing hydrolysis seen with the amino acid substrates should not interfere with the efficiency of the elimination with other carboxylic acids. As anticipated, when the elimination of **3b** was performed with one equivalent of water, a comparable yield was observed (Table 3, Entry 2).

The possibility of an *in situ* reduction of the cobaloxime was also explored in order to eliminate the need for a pre-reduction step. Both **1a** and **3b** were subjected to the reaction conditions in which all reagents were added just before the onset of irradiation (see Experimental Section *in situ* reduction procedure for details). To our delight, comparable yields of **2a** and **4b** were obtained (Table 3, Entry 3 & 6). In contrast, when the reaction was run in the absence of the reductant, a ~20% decrease in the yield was observed (Table 3, Entry 7). Additionally, a reaction performed without any water or base resulted in a large yield reduction compared with optimal conditions (Table 3, Entry 8).

Table 3: Evaluation of reaction conditions

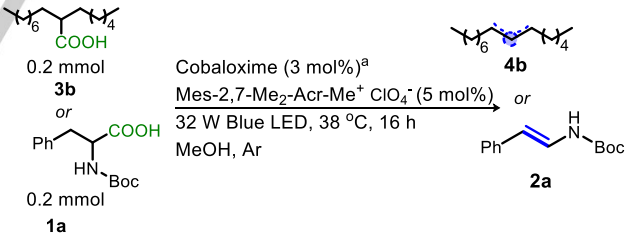

Entry & Acid	Additives	Yield[b]
1 **3b**	STAB (7.5 mol%), Na_2CO_3 (1 mol %), H_2O (7.5 mol %)	88% **4b**
2 **3b**	STAB (7.5 mol%), Na_2CO_3 (1 mol %), H_2O (100 mol %)	93% **4b**
3 **3b**	STAB (7.5 mol%), Na_2CO_3 (1 mol %), H_2O (7.5 mol %)	83% **4b**[c]
4 **3b**	STAB (7.5 mol%), Na_2CO_3 (100 mol %), H_2O (7.5 mol %)	26% **4b**
5 **1a**	STAB (7.5 mol%), Na_2CO_3 (1 mol %), H_2O (7.5 mol %)	93% **2a**
6 **1a**	STAB (7.5 mol%), Na_2CO_3 (1 mol %), H_2O (7.5 mol %)	86% **2a**[c]
7 **1a**	Na_2CO_3 (1 mol%), H_2O (7.5 mol %)	74% **2a**
8 **1a**	STAB (7.5 mol %)	46% **2a**
9 **1a**	H_2 [d], Na_2CO_3 (0.1 mol %), H_2O (7.5 mol %)	13% **2a**[e]

[a] Co(dmgH)$_2$ClPy for **1a**; Co(dmgH)$_2$Cl(*N*-Me-Imidazole) for **3b**.[b] Isolated yields. [c] Reduction of the Co was performed *in situ* in entries 3 & 6 and pre-reduction method utilized in entries 1-2, 4-5, 7-9. [d] Co(dmgH)$_2$ClPy in 0.5 mL MeOH was sparged with 10% H_2/N_2 for 1 h before being subjected to reaction conditions. [e] Yield determined by q^{1}H NMR with pyridine (0.2 mmol) as the internal standard.

Interestingly, while the presence of 1 mol % Na_2CO_3 aids in providing optimal yields, one equivalent of base was detrimental to the reactions success (Table 3, Entry 4). This stands in stark contrast to the Ritter methodology, where stoichiometric base did not change to the observed yield and led to improved reaction rates.[3b] However, the Heck-type methodology of Liu/Wu (Scheme 1E) does benefit from the use of a catalytic amount of base. Presumably, the base is generating the carboxylate reductant and could also help establish an equilibrium between Co(III) hydride and Co(I).[3d]

Lastly, the propensity for STAB to react with methanol and form H_2 was not overlooked.[19] The high success of STAB compared to the other reductants screened ($NaBH_4$, $NaCNBH_3$) was initially attributed to STAB being a comparably mild reductant. To see if the ability of STAB to generate H_2 in methanol was involved in the making of the active catalyst, the cobalt catalyst was sparged with H_2 before being subjected to the reaction. However, the standard yellow to red color change (Figure 7A) was not observed and its performance in the elimination was low (Table 3, Entry 9). Ultimately, the comparable performance between STAB and Zn

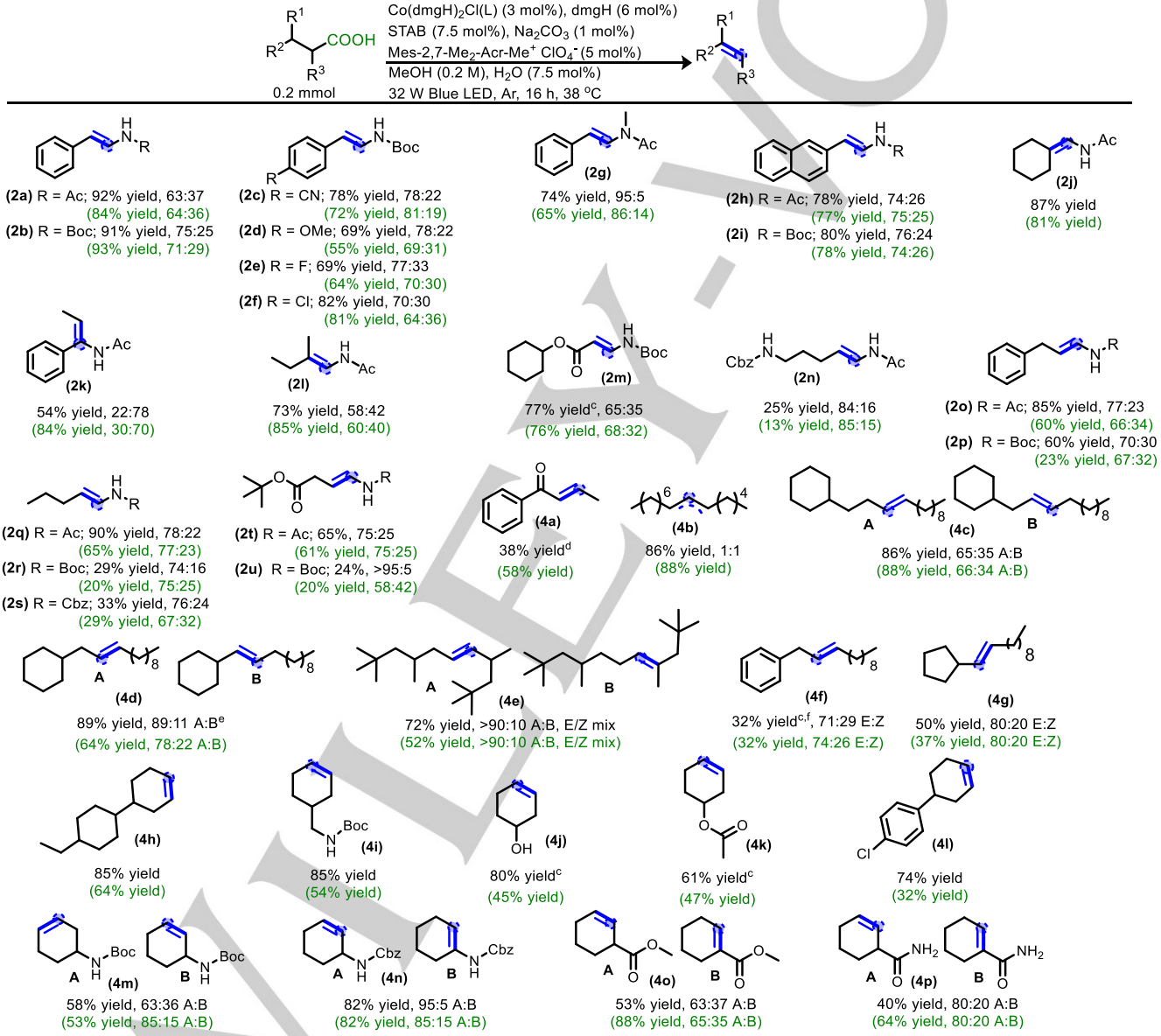

Table 4: Elimination with excess dmgH ligand

[a] Pre-reduction procedure with $Co(dmgH)_2ClPy$ was utilized for **2a-u**. *In situ* reduction procedure with $Co(dmgH)_2Cl$(*N*-Me-Imidazole) was utilized for **4a-p** (see Experimental Section for details). [b] Isolated yields are reported unless otherwise specified; reported ratios for enamide products are E:Z isomer ratios determined by ^1H NMR. [c] q^1H NMR yield with 0.2 mmol pyridine as the internal reference standard. [d] Isolated only the *E*-isomer; reaction produces >99:1 E:Z. [e] >95:5 E:Z. [f] Isolated with alkane and in >95:5 regioisomer ratio. [g] COSY used to determine regioisomer ratio. [h] NOESY used to determine geometric isomers. [i] () yields are without extra ligand.

has led us to believe that STAB serves as a reductant, possibly aiding in the formation of an active catalytic species from the cobaloxime pre-catalyst.[3c]

Finally, additives were examined in attempt to address the observation that some reactions, particularly with the non-amino acids, did not reach full conversion. As discussed in the "Catalyst Influence" Section 2.1.3, catalyst stability appears to be positively correlated with the yields of olefin product observed. Thus, the lack of complete conversion was posited to be a result of catalyst degradation. To address this, recharging the reactions with fresh catalyst was attempted, but this did not improve the yield of elimination (Table S2). In fact, when more photocatalyst or more cobaloxime was added before the 16-hour completion time, the reaction proceeded to even lower conversion. When the reaction solution was charged with both photocatalyst and cobaloxime simultaneously, the reaction was not inhibited but the alkene yield did not improve.

The limitation in conversion was ultimately overcome through the addition of excess oxime ligand to the reaction mixture. Delightfully, this addition of dimethylglyoxime (dmgH, 6 mol%) to the reaction led to significant yield improvements in most cases, particularly for those that suffered from low conversion (Table 4). This is consistent with the findings of Eisenberg in studies of Eosin Y and $Co(dmgH)_2ClPy$ water oxidation systems.[20] They suggested that catalyst degradation is a result of the labile dmgH and found that this degradation can be counteracted through the addition of excess dmgH. Presumably, the excess ligand aids in ensuring the cobaloxime remains appropriately ligated, thus improving catalyst longevity (Table 4).

2.4 Side Product Evaluation

2.4.1 Aminal Byproduct

In the development of this elimination protocol, amino acids underwent decarboxylative olefin formation cleanly and with high efficiency. However, an aminal byproduct, derived from methanol addition, was a consistent side product that was typically formed in < 10% yield (Scheme 3). We expect that this product could be arising from nucleophilic addition of the methanol solvent to an imine or iminium species generated either through HAT from N–H or through oxidation of the carbamate by the photocatalyst.[21]

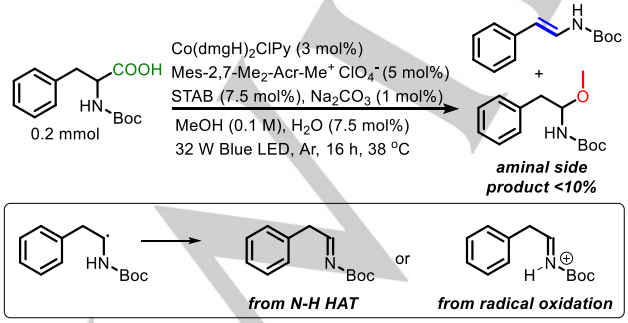

Scheme 3: Aminal side product

2.4.2 Alkane Byproduct

Although aliphatic acids don't produce the methoxy addition product, a saturated alkane byproduct is observed in most cases. While the imidazole-ligated catalyst does not generate much alkane under our normal room temperature conditions, alkane formation was particularly problematic when higher intensity blue LED lamps were utilized without cooling. Under such conditions, the reaction temperature could be increased to 95 °C. As a result of the higher intensity irradiation, the elimination of **3b** proceeded at a faster rate, reaching completion in 4 hours; however, the competing production of reduced alkane becomes more prevalent (Scheme 4). We hypothesized that this side product could be a result of one of the following pathways: 1) a disproportionation between alkyl radical intermediates,[22] or 2) a hydrogenation of the alkene with cobalt and H_2.[23]

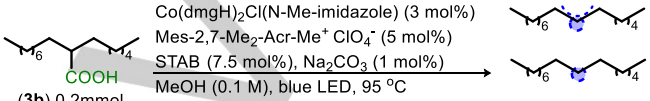

Time (hrs)	*alkene:alkane (GC/MS ratio)*
4	93:7
8	86:14
16	82:18
24	68:32
72	68:32

Scheme 4: Elimination at elevated temperature

Evaluation of the alkane formation under normal, room temperature conditions was accomplished using acid **3l** since cyclic substrates typically provided greater quantities of saturated product than the acyclic examples. This evaluation revealed that the alkane product does not begin appearing until late in the reaction (Scheme 5). When the reaction was irradiated for an extended period of time, the quantity of alkane relative to alkene continues to increase until a 60:40 alkene:alkane ratio is reached.[24] The delayed production of alkane likely indicates that the alkane formation results from a decomposed cobalt catalyst that is either an effective hydrogenation catalyst or is ineffective at HAT, which leads to greater disproportionation at later reactions times.

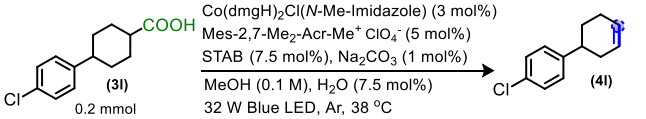

Irradiation Time	**Alkane:Alkene (%)**
6 h	0:42
12 h	10:62

Scheme 5: Alkane formation

[a] Product ratios observed by GC/MS. [b] *In situ* reduction protocol followed.

In addition, it is interesting to note that the changes in cobaloxime also led to changes in the amount of alkane observed (Table 5). In assessment of the equatorial ligand changes, it is worth noting that the quantity of alkane relative to alkene was greatest with the chgH ligand, followed by dmgH. The lowest quantity of alkane was observed with the dpgH; however, these catalysts also led to lower conversion. The identity of the axial ligand also influences

the alkene:alkane ratio. Notably, the least amount of alkane arises when the *N*-Me-imidazole is utilized as the axial ligand. As discussed in Section 2.1, this is the axial ligand that provides the cobaloxime with the greatest stability.[12a] Again, this suggests that a poorly stable catalyst gives rise to more alkane product at later reaction times when catalyst degradation would be most significant.

To further investigate the mechanism of alkane formation, the elimination of **3b** was investigated using a poorly selective Co(dmgH)$_2$Cl(*N*-Me-benzimidazole) catalyst (Scheme 6A). In order to determine if the hydrogen that is evolved leads to hydrogenation of the alkene, gaseous H_2 was continuously removed by maintaining a flow of nitrogen through the head-space of the reaction vessel. Under these conditions, the elimination provided product **4b** in 58% yield and a 77:23 alkene:alkane ratio (Scheme 6B). This result is an improvement over the standard reaction conditions (39% yield, 60:40 alkene:alkane ratio, Scheme 6A). Thus, the lower quantity of alkane produced under these modified conditions indicates that the increasing [H_2] plays a role in the production of alkane.

Table 5: Catalyst influence on alkane formation

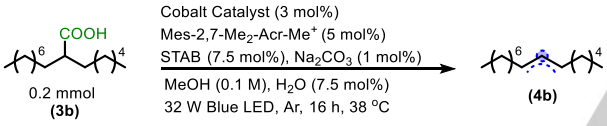

Cobalt Catalyst	GC/MS: Alkene	Alkane	Acid	Yield (8e)
Co(chgH)$_2$ClPy	44%	51%	4%	29%
Co(chgH)$_2$Cl(DMAP)	36%	19%	45%	(22%)
Co(chgH)$_2$Cl(*N*-Me-Imidazole)	74%	12%	14%	56%
Co(chgH)$_2$Cl(1,2-dimethylimidazole)	40%	27%	33%	(31%)
Co(chgH)$_2$Cl(*N*-Me-Benzimidazole)	33%	37%	30%	(26%)
Co(dmgH)$_2$ClPy	71%	14%	16%	63%
Co(dmgH)$_2$Cl(4-iPr-Py)	68%	26%	6%	(55%)
Co(dmgH)$_2$Cl(DMAP)	45%	23%	32%	(50%)
Co(dmgH)$_2$Cl(4-Cl-Py)	21%	30%	49%	(3%)
Co(dmgH)$_2$Cl(*N*-Me-Imidazole)	95%	5%	0%	88%
Co(dmgH)$_2$Cl(1,2-dimethylimidazole)	56%	30%	14%	(41%)
Co(dmgH)$_2$Cl(*N*-Me-Benzimidazole)	59%	39%	2%	(39%)
Co(dmgH)$_2$Cl(PPh$_3$)	32%	33%	35%	(32%)
Co(dpgH)$_2$ClPy	18%	13%	69%	(7%)
Co(dpgH)$_2$Cl(4-iPr-Py)	32%	12%	56%	(28%)
Co(dpgH)$_2$Cl(*N*-Me-Imidazole)	28%	0%	72%	34%
Co(dpgH)$_2$Cl(1,2-dimethylimidazole)	23%	28%	49%	(15%)

[a] Product ratios were determined by GC/MS. [b] (yields) were determined by q^{1}H NMR using 0.2 mmol pyridine as the internal reference standard. All other yields isolated.

Next, to investigate the role of catalyst stability in alkane formation, the reaction was performed with additional dmgH which slows degradation of the cobalt catalyst. This led to a significant improvement in alkene yield (76%) and a decrease in the amount of alkane side product produced (82:18 alkene:alkane, Scheme 6C).

A. Standard Decarboxylative Elimination Conditions

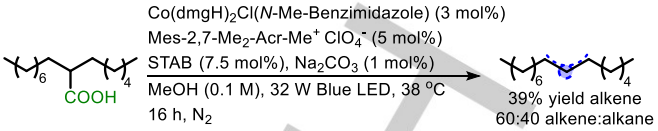

B. Elimination with Removal of Gaseous Side-Products

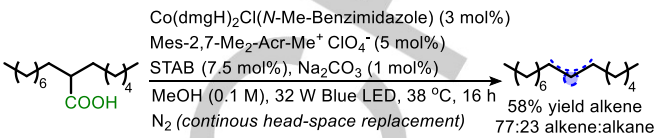

C. Elimination with Additional dmgH Ligand

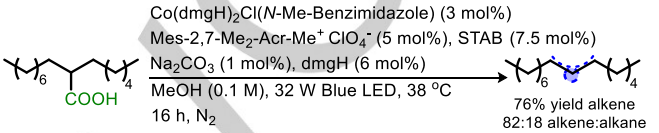

Scheme 6: Formation of alkane under modified reaction conditions [a] Reported yields were determined by q^{1}H NMR with pyridine internal standard. [b] Reported product ratios were determined by GC/MS of the crude reaction mixture.

Taken together, these experiments point to a catalyst degradation pathway that forms a cobalt catalyst that is more effective at hydrogenation of alkenes. This is supported by the delayed onset of alkane formation and explains why more stable catalysts provide higher alkene:alkane product ratios.[12a]

2.5 Mechanistic Assessment

Several mechanistic pathways need to be considered to access the dominant catalytic pathway. First, it is important to note that the decarboxylative elimination does *not* proceed without both the photocatalyst and the cobaloxime catalyst.[3c] As such, the acridinium is expected to operate via a single electron oxidation of the carboxylate and re-oxidation of the reduced photocatalyst is facilitated by the cobaloxime. The cobaloxime is further thought to be involved in the deprotonation event, HAT, and ultimately hydrogen evolution. Extensive studies of the cobaloxime species have been reported and several relevant plausible pathways have arisen from these reports (Figure 7).[25]

2.5.1 Catalytically Active Co Oxidation States

The mechanism proposed in our initial report was centered around a cycle that employed Co(III), Co(II), and Co(I).[3c] In this proposal, the super nucleophilic Co(I) species serves as the base to deprotonate the carboxylic acid and the resulting cobalt hydride would be involved in the HAT and subsequent HE event (eq. 1 & 2).[26]

$$Co(I)^{\ominus} + HA \longrightarrow Co(III)\text{-}H + A^{\ominus} \quad (1)$$

$$Co(II)\text{-}H^{\bullet-} + \text{alkyl radical} \longrightarrow Co(I)^{\ominus} + H_2 + \text{alkene} \quad (2)$$

However, further investigation into the cobalt species that results from our pre-reduction led us to re-evaluate the presence of an anionic Co(I). The initial indication that our pre-catalyst was not

Co(I) was the red color observed after treatment with sodium triacetoxyborohydride. Co(I) is typically reported to be blue, blue-green, or purple in color; this is a stark difference from the observed red pre-catalyst solution (Figure 7A).[25b,26] A more rigorous UV-vis analysis of the pre-catalyst revealed an absorbance that is more fitting for a solution that is a Co(II) or Co(III) species (Figure S9). In addition, a Co(I) species should be easily alkylated with alkyl halides, however, no alkylation was observed when methyl iodide was added to the red cobalt solution (Figure 7B).[27,28]

A. Comparison of Cobaloxime Pre-Catalyst to Co(I)

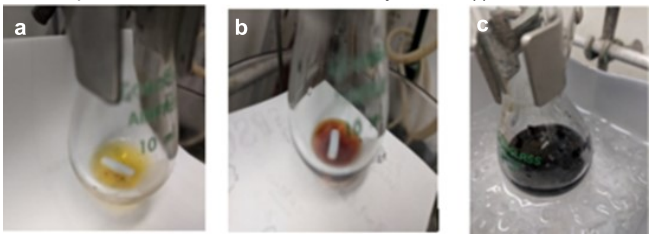

[a] initial cobaloxime. [b] after reduction. [c] independently generated Co(I) using $NaBH_4$ in rigorously degassed MeOH.

B. Attempted Alkylation of Cobaloxime Pre-Catalyst

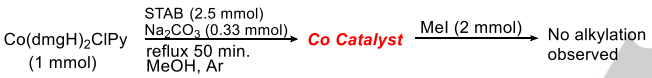

Figure 7: Evaluation of cobaloxime pre-catalyst

Although Co(I) is not likely the pre-catalyst for decarboxylative elimination chemistry, it is important to note that the use of a reductant (STAB or Zn) leads to higher yields (Table 3, entry 6).[3c] Thus, the reductant may aid in accessing a more active form of the catalyst at the onset of the reaction. It has been suggested that borohydride reductants often lead to Co(II) species instead of Co(I) as a result of a reactive Co(III) hydride undergoing bimetallic hydrogen evolution (eq. 3).[29]

$$\text{Co(III)-H + Co(III)-H} \longrightarrow \text{2 Co(II) + } H_2 \qquad (3)$$

Thus, our reaction conditions could be allowing for an expedited formation of a catalytically active Co(II) species. To this end, we favor a pathway where a Co(III) hydride is initially generated through HAT to Co(II), and hydrogen evolution is achieved via protonation of either a Co(III) hydride or a Co(II) hydride (eq. 4-6). The Co(III)/(II) cycle is in agreement with the mechanism proposed by Ritter.[3b]

HAT Pathway:

$$\text{Co(II) + alkyl radical} \longrightarrow \text{Co(III)-H + alkene} \qquad (4)$$

HE Pathways:

$$\text{Co(III)-H + HA} \longrightarrow \text{Co(III)}^{\oplus} + H_2 + A^{\ominus} \qquad (5)$$

$$\text{Co(II)-H}^{\cdot-} + \text{HA} \longrightarrow \text{Co(II) + } H_2 + A^{\ominus} \qquad (6)$$

2.5.2 Cobalt Alkyl Complex

The suspected catalytically active Co(II) species may form a formal Co(III)–C off-cycle intermediate that will need to homolyze under the reaction conditions for catalysis to proceed. Ritter reported an experiment in which stoichiometric alkyl cobaloxime was subjected to their reaction conditions. They observed that the alkyl ligand underwent the elimination, a result which supports a pathway in which a Co(III)–C bond can be homolyzed and subsequent HAT process can allow for catalysis to proceed.[3c,30] To further explore this pathway under our conditions, Co(dmgH)$_2$(*n*-butyl)Py was synthesized and employed as a catalyst in the reaction. Here the homolysis would provide the Co(II) species that is anticipated to be the catalytically active species that initiates the decarboxylative elimination. The Co(II) species generated via homolysis could further perform HAT from the butyl radical to become a catalytically active Co(III) hydride (Scheme 7A). Indeed, the reaction of *N*-Boc phenylalanine employing the Co(dmgH)$_2$(*n*-butyl)Py as a catalyst provided a 58% yield of enecarbamate. Thus, under our reaction conditions, radicals that are stored as off-cycle, persistent cobalt alkyl complexes can readily reenter the cycle (Scheme 7B).

A. Photolysis of Co(dmgH)$_2$(*n*-butyl)Py

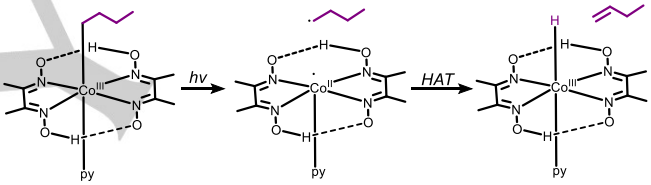

B. Decarboxylative Elimination with Co(dmgH)$_2$(*n*-butyl)Py

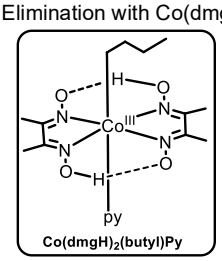

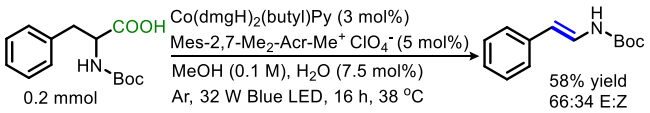

Scheme 7: Reaction with alkyl cobaloxime catalyst

As mentioned, homolysis of cobalt-alkyl species leads to radicals that can undergo elimination via HAT. The rate of this HAT was further probed by competition reactions performed in the presence of one equivalent of TEMPO. Photolysis of a cobalt n-nonyl complex along with TEMPO produced a 40:60 ratio of alkene to TEMPO-trapped products (Scheme 8A). These results indicate that the HAT process is occurring at a rate that is comparable to the bimolecular radical coupling of the alkyl radical intermediate and TEMPO (~1.5 x 10^8 $M^{-1}s^{-1}$).[31] A similar ratio of products is observed in a catalytic reaction with an α,α-disubstituted carboxylic acid (Scheme 8B).[32]

A. TEMPO in Cobalt-Alkyl Homolysis

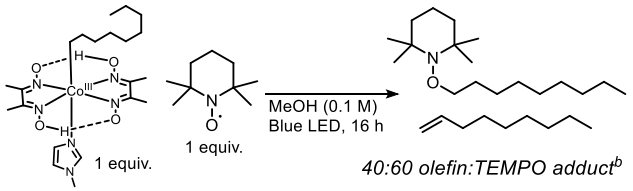

B. TEMPO in Decarboxylative Elimination

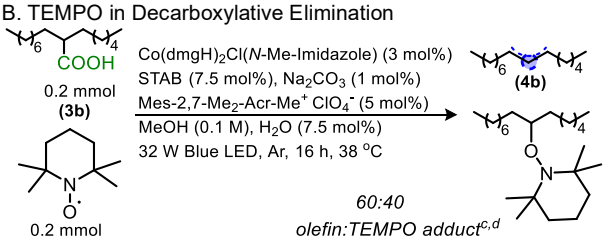

Scheme 8: Elimination vs. TEMPO trapping

[a] *In situ* reduction protocol followed (see Experimental Section for details). [b] Products were isolated separately. [c] Products were isolated together, and the product ratio was determined by GC/MS of the crude reaction mixture. [d] Product ratio shown is an average of three reactions.

2.5.3 Electron and Proton Transfer Pathways

While the stoichiometric photolysis of Co-alkyl complexes is strong evidence that alkene formation by HAT is possible, it is important to note that a pathway in which the alkyl radical intermediate is further oxidized to a cation followed by deprotonation to furnish the alkene is also plausible. This oxidation has been previously proposed to be facilitated by Co(II) with deprotonation occurring from the resulting anionic Co(I).[8a,33] However, the reduction potentials for the aliphatic radicals are >0 V vs. SCE,[34] whereas both the Co(III)/(II) and Co(II)/(I) potentials (-0.68 V and -1.13 V, respectively)[25b] are too low for this SET to be favorable. Thus, if such radical-polar crossover occurs through oxidation, only the acridinium catalyst employed is sufficiently oxidizing. While possible, such oxidation to a cation would lead to E1-type elimination which is not consistent with the preferred formation of less-substituted alkenes, nor is it consistent with the catalyst-dependent regioselectivities for elimination. Alternatively, our observed reaction profile is fully consistent with Muckerman's suggestion that HAT to form Co(III)-H from Co(II) through a PCET pathway is part of the lowest energy pathway *en route* to cobaloxime-facilitated hydrogen evolution.[35] Thus, a PCET pathway is most likely involved.

From the aforementioned experiments, it became apparent that the dominant cycle likely operates through Co(II) and Co(III) and appears to have similarities to studies on the cobalt-catalyzed hydrogen evolution using photoacids.[36] As supported by these reports, two pathways are possible for the subsequent monometallic hydrogen evolution process that result in the deprotonation event (eq. 5 & 6). The Co(III) hydride can be reduced first by the photocatalyst to provide Co(II) hydride and then hydrogen evolution through protonation of this hydride with carboxylic acid would give Co(II) and the carboxylate [the Co(III)-H reduction potential is reported to be similar to Co(II)/(I) reduction, ~-1.0 V vs. SCE].[20a,25,37] Alternatively, the Co(III) hydride can perform hydrogen evolution by protonation with acid. In this event, the resulting $Co(III)^+$ (~-0.68 V vs. SCE)[25] would then be reduced by the photocatalyst to form Co(II) and close the catalytic cycle. We favor the latter hydrogen evolution that involves the Co(III) hydride and carboxylic acid because the potential of the acridinium photocatalyst (~-0.6 V vs SCE)[9] is more suited for the reduction of $Co(III)^+$ as opposed to the reduction of Co(III) hydride (eq. 5 & 6).[29]

2.5.4 Proposed Decarboxylative Elimination Pathway

Taken together, a mechanistic picture to better describe the dominant catalytic cycle was devised (Scheme 9). Here, the cycle is initiated by single electron oxidation of the carboxylate (generated by the catalytic base) with the photoexcited acridinium catalyst, which triggers rapid decarboxylation. The alkyl radical is then trapped by Co(II) through HAT to furnish Co(III) hydride and the desired alkene. The Co(III) hydride then deprotonates a molecule of carboxylic acid, evolving hydrogen gas, and becoming $Co(III)^+$. The $Co(III)^+$ can undergo single electron reduction by the photocatalyst, which closes the catalytic cycle of both the Co and photocatalyst.

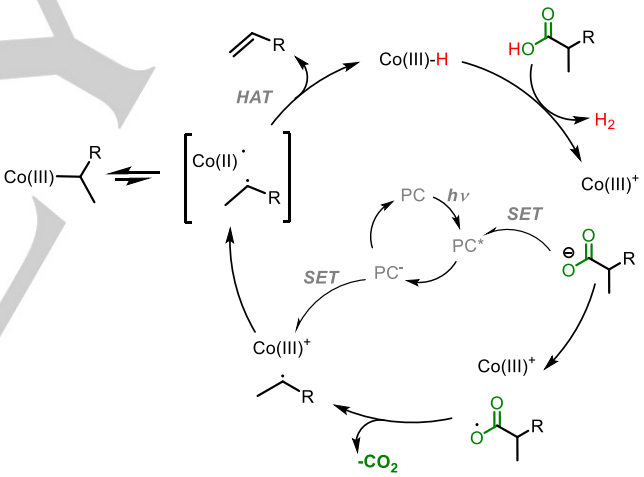

Scheme 9: Hypothetical Mechanism

3. Conclusions

Herein, the development and mechanistic evaluation of the photoredox/cobaloxime dual catalytic decarboxylative elimination have been described. This combination of decarboxylation and hydrogen evolution has allowed for the direct decarboxylative process to proceed with no stoichiometric additives under mild and neutral conditions efficiently and with high atom economy.

The Fukuzumi class of acridinium catalysts has been found to provide the best results, with the slightly less oxidizing but more reducing Mes-2,7-Me_2-Acr-Me^+ ClO_4^- providing higher yields for the non-amino acid examples compared to the Mes-2,7-Me_2-Acr-Ph^+ BF_4^- employed in the first-generation method.

The optimal cobaloxime catalyst for the amino acids was identified to be the $Co(dmgH)_2ClPy$, however, these substrates eliminate well with a variety of cobaloximes. Conversely, other carboxylic acid substrates underwent elimination most effectively when $Co(dmgH)_2Cl$(*N*-Me-Imidazole) was utilized as the co-catalyst. Importantly, reaction efficiency can be maximized, and the reaction scope expanded, by improving the catalyst longevity via appropriate choice of axial base ligand and through the addition of extra dmgH ligand.

Observations also point to the HAT process requiring the cobaloxime catalyst to be in close proximity to the reaction site and, as such, sterically encumbered substrates and ligands detract from the reaction efficiency. One artifact of the steric influences on the elimination is the preference for the less thermodynamically favored Hofmann products and less sterically encumbered alkene products. The regioisomer ratios observed have been shown to be kinetic ratios that are established during the elimination and not a result of subsequent isomerization.

From our studies, we believe the dominant catalytic cycle employs Co(II) and Co(III) intermediates and not an anionic Co(I) species. In addition, an evaluation of potentials has led to the conclusion that a PCET pathway is the preferred route for HAT, and HE via protonation of the Co(III) hydride is the most likely pathway.

In sum, the methodology reported herein can be employed for the synthesis of alkenes from a variety of carboxylic acids. We anticipate that our observations and conclusions will aid in the utilization of this methodology as well as the future development and understanding of similar dual catalytic processes.

4. Experimental Section

General Considerations:

Purification was accomplished with column chromatography using silica gel (60 Å porosity, 230 x 400 mesh, standard grade) which was purchased from Sorbent Technologies (catalog # 30930M-25). TLC analysis was performed (fluorescence quenching and potassium permanganate acid stain) with silica gel HL TLC plates with UV254 purchased from Sorbent Technologies. ^1H and ^{13}C NMR spectra were obtained on a Bruker ADVANCE 500 DRX equipped with a QNP cryoprobe. These spectra were referenced to residual protio solvent signals. HRMS data was obtained on an ESI LC-TOF Micromass LCT (Waters). HRMS data was collected using ESI mass spectrometry. Melting points were obtained with Digimelt MPA 160 SRS (# 111278) and samples were loaded with borosilicate glass Kimble tube capillaries (# 34505-9a). GC/MS data was acquired on Shimadzu GCMS-QP2010 SE. UV-visual data was acquired with Ocean Optics DT-MINI-2-GS.

All *N*-Boc and *N*-Cbz amino acids are commercially available and were used without further purification. *N*-Acetyl amino acids, 1-[(1,1-dimethylethoxy)carbonyl]-L-prolyl-L-phenylalanine, *N*-acetyl-norleucine, and *N*-acetyl-glutamic acid are commercially available and were used without further purification. All non-protected amino acids utilized are commercially available and were used without further purification. The acyl protected variants were previously made in our lab.[3c] Carboxylic acids (**3a,3b,3e,3h-3o**) are commercially available and were used without further purification. Sodium triacetoxyborohydride was purchased from Oakwood. Photocatalysts 9-mesityl-10-phenylacridinium tetrafluoroborate, 9-mesityl-10-methyllacridinium perchlorate, 9-mesityl-2,7-dimethyl-phenylacridinium tetrafluoroborate, and 9-mesityl-3,6-(*t*Bu)$_2$-10-phenylacridinium tetrafluoroborate were purchased from Sigma-Aldrich. Photocatalyst 9-mesityl-10-methylacridinium perchlorate and 9-mesityl-2,7-Me$_2$-10-methylacridinium perchlorate was purchased from TCI. Cobaloxime, $Co(dmgH)_2ClPy$, was purchased from Sigma-Aldrich. Other cobaloximes were synthesized using $CoCl_2$ from ChemImpex and the respective oxime ligands all purchased from Sigma-Aldrich. All axial base ligands used were commercially available. Anhydrous MeOH was purchased from Acros.

Final decarboxylative elimination reactions were run in a screw-threaded tube from Chemglass (CLS-4208). Kessil H150 Blue LED grow lights provided 450 nm light. Two lights were used in the set-up of these reactions (see Supporting Information Figure S1 and S2 for images and further description of photoredox reaction set-up). A 2.0 mL solution of MeOH had an internal temperature of 38 °C after 1 hour under standard reaction conditions.

General Procedure for the Synthesis of Cobaloximes:

Modified from literature procedure.[28] To a 100 mL round-bottom flask with stir bar, $CoCl_2$ hydrate (2.3 mmol, 0.54 g) and acetone (15 mL) were added and stirred resulting in a blue homogeneous solution. To this solution, the respective oxime ligand (7.5 mmol) was added and the color changed from blue to purple/pink. Air was passed over this solution via an air inlet line made from Tygon tubing and a 1 mL syringe. Fresh acetone was added when solution became concentrated to maintain constant volume (15 mL). After ~0.5-1 hour, a green precipitate formed. The reaction mixture is cooled to 0 °C and the green solid was filtered via vacuum filtration, then washed with ~10 mL diethyl ether. This solid was then added to a 100 mL round-bottom flask with stir bar and taken up in MeOH (20 mL). To the stirring solution, the respective base ligand was added (4.05 mmol) and the solution turned brown immediately. The reaction mixture was allowed to stir for 30 min. After, stirring is stopped and the mixture was cooled to 0 °C. The resulting brown solid was collected via vacuum filtration and washed with water (~10 mL) then diethyl ether (~10 mL). The product was dried under vacuum to yield the desired cobaloxime. The cobaloxime complexes were then utilized without further purification.

Co(chgH)$_2$Cl(DMAP) isolated as brown solid in 57% yield. ^1H NMR (500 MHz, CD_3CN): δ 7.44 (d, 2H), 6.43 (d, 2H), 2.96-2.86 (m, 4H), 2.92 (s, 6H), 2.81-2.68 (m, 4H), 1.76-1.58 (m, 8H). ^{13}C NMR (126 MHz, CD_3CN): δ 153.8, 149.3, 109.1, 39.4, 26.7, 22.1. IR (film): 3445, 3055, 2989, 1687, 1636, 1608, 1422, 763, 749, 653 cm^{-1}. HRMS: Calc'd $C_{19}H_{29}N_6O_4ClCo$ (M+H) = 499.1271, found 499.1291.

Co(chgH)$_2$Cl(Py) isolated as brown solid in 56% yield. ^1H NMR (500 MHz, CD_3CN): δ 8.11 (d, 2H), 7.79 (t, 1H), 7.30 (t, 2H), 2.97-2.87 (m, 4H), 2.81-2.69 (m, 4H), 1.75-1.58 (m, 8H). ^{13}C NMR (126 MHz, CD_3CN): δ 154.5, 151.7, 140.4, 126.8, 26.8, 22.0. IR (film): 3403, 3006, 2945, 1670, 1665, 1422, 763, 701, 638 cm^{-1}. HRMS: Calc'd $C_{17}H_{24}N_5O_4ClCo$ (M+H) = 456.0849, found 456.0830.

Co(chgH)$_2$Cl(1,2-dimethylimidazole) isolated as a light brown solid in 97% yield. ^1H NMR (500 MHz, CD_3CN): δ 7.37-7.29 (m, 13H), 7.25-7.19 (m, 7H), 7.00 (d, 1H), 6.84 (d, 1H), 3.51 (s, 3H), 2.45 (s, 3H). ^{13}C NMR (126 MHz, CD_3CN): δ 154.3, 131.2. 130.7, 130.6, 130.4, 128.9, 128.8, 127.1, 122.5, 35.0, 11.5. IR (film): 3400, 3055, 2987, 1651, 1634, 1423, 750, 705, 638 cm^{-1}. HRMS: Calc'd $C_{17}H_{27}N_6O_4ClCo$ (M+H) = 473.1114, found 473.1137.

Co(chgH)$_2$Cl(N-Me-Imidazole) isolated as brown solid in 10% yield. ^1H NMR (500 MHz, CD_3CN): δ 7.15 (s, 1H), 6.83 (s, 1H), 6.49 (s, 1H), 3.55 (s, 3H), 2.93-2.84 (m, 4H), 2.84-2.74 (m, 4H), 1.78-1.62 (m, 8H). ^{13}C NMR (126 MHz, CD_3CN): δ 153.5, 139.4, 128.0, 123.6, 35.5, 26.7, 22.1. IR (film): 3409, 3054, 2987, 1674, 1657, 896, 750, 639 cm^{-1}. HRMS: Calc'd $C_{16}H_{25}N_6O_4ClCo$ (M+H) = 459.0958, found 459.0973.

Co(chgH)$_2$Cl(N-Me-Benzimidazole) isolated as a tan solid in 23% yield. ^1H NMR (500 MHz, CD_3CN): δ 8.15 (d, 1H), 7.88 (s, 1H), 7.42 (d, 1H), 7.37-7.26 (d, 2H), 3.76 (s, 3H), 2.97-2.87 (m, 4H), 2.76-2.66 (m, 4H), 1.73-1.63 (m, 4H), 1.63-1.53 (m, 4H). ^{13}C NMR (126 MHz, CD_3CN): δ 153.4, 145.1,

124.2, 123.6, 111.1, 31.9, 25.8, 21.1. HRMS: Calc'd $C_{20}H_{27}N_6O_4ClCo$ (M+H) = 509.1114, found 509.1119.

Co(dmgH)$_2$Cl(PPh$_3$) isolated as chocolate brown solid in 12%* yield (*contains additional PPh_3). ^{1}H NMR (500 MHz, CD_3CN): δ 7.44-7.34 (m, 15H), 1.99 (s, 6H), 1.98 (s, 6H). ^{13}C NMR (126 MHz, CD_3CN): δ 153.7, 135.1, 135.0, 132.5, 129.4, 129.3, 13.0. IR (film): cm^{-1}. HRMS: Calc'd $C_{26}H_{29}N_4O_4PClCo$ (M+) = 586.0947, found 586.0931.

Co(dmgH)$_2$Cl(DMAP) isolated as orange/brown solid in 78% yield. ^{1}H NMR (500 MHz, CD_3CN): δ 7.45 (d, 2H), 6.42 (d, 2H), 2.91 (s, 6H), 2.31 (s, 12H). ^{13}C NMR (126 MHz, CD_3CN): δ 152.3, 148.5, 108.3, 38.6, 12.1. IR (film): 3435, 3004, 2945, 1647, 1622, 1436, 1374, 920, 639 cm^{-1}. HRMS: Calc'd $C_{15}H_{24}N_6O_4ClCo$ (M+) = 446.0880, found 446.0893.

Co(dmgH)$_2$Cl(4-iPr-Py) isolated as brown solid in 78% yield. ^{1}H NMR (500 MHz, CD_3CN): δ 7.97 (d, 2H), 7.17 (d, 2H), 2.86 (q, 1H), 2.31 (s, 12H), 1.13 (d, 6H). ^{13}C NMR (126 MHz, CD_3CN): δ 162.7, 153.7, 151.2, 125.1, 33.9, 22.7, 13.0. IR (film): 3397, 3041, 2945, 1652, 1635, 1374, 639 cm^{-1}. HRMS: Calc'd $C_{16}H_{26}N_5O_4ClCo$ (M+H) = 446.1005, found 446.1009.

Co(dmgH)$_2$Cl(4-Cl-Py) isolated as orange solid in 70% yield. 4-Cl-Py HCl was basified with sodium carbonate and extracted with DCM before use. ^{1}H NMR (500 MHz, CD_3CN): δ 8.03 (d, 2H), 7.35 (d, 2H), 2.32 (s, 12H). ^{13}C NMR (126 MHz, CD_3CN): δ 154.0, 152.5, 126.9, 13.0. IR (film): 3390, 3055, 2987, 1670, 1652, 749, 705, 638 cm^{-1}. HRMS: Calc'd $C_{13}H_{29}N_5O_4Cl_2Co$ (M+H) = 448.0929, found 448.0918.

Co(dmgH)$_2$Cl(1,2-dimethylimidazole) isolated as orange/brown solid in 66% yield. ^{1}H NMR (500 MHz, CD_3CN): δ 6.79 (d, 1H), 6.68 (d, 1H), 3.36 (s, 3H), 2.33 (s, 12H), 2.19 (s, 3H). ^{13}C NMR (126 MHz, CD_3CN): δ 153.3, 127.5, 121.7, 34.7, 12.9, 11.2. IR (film): 3391, 3005, 2944, 1644, 1637, 1374, 639 cm^{-1}. HRMS: Calc'd $C_{13}H_{23}N_6O_4ClCo$ (M+H) = 421.0801, found 421.0822.

Co(dmgH)$_2$Cl(N-Me-Imidazole) isolated as light brown solid in 69% yield. ^{1}H NMR (500 MHz, CD_3CN): δ 7.14 (s, 1H), 6.81 (t, 1H), 6.49 (t, 1H), 3.54 (s, 3H), 2.32 (s, 12H). ^{13}C NMR (126 MHz, CD_3CN): δ 156.0, 152.8, 137.8, 127.5, 31.7, 12.9. IR (film): 3387, 3055, 2987, 1656, 1634, 1422, 896, 748, 639 cm^{-1}. HRMS: Calc'd $C_{12}H_{21}N_6O_4ClCo$ (M+H) = 407.0645, found 407.0630.

Co(dmgH)$_2$Cl(N-Me-Benzimidazole) isolated as orange/brown solid in 80% yield. ^{1}H NMR (500 MHz, CD_3CN): δ 8.17 (d, 1H), 7.88 (s, 1H), 7.40 (d, 1H), 7.31 (m, 2H), 3.75 (s, 3H), 2.29 (s, 12H). ^{13}C NMR (126 MHz, CD_3CN): δ 153.7, 146.0, 125.0, 124.6, 112.1, 32.9, 13.0. IR (film): 3536, 3004, 2945, 1641, 1614, 1435, 1375, 919, 639 cm^{-1}. HRMS: Calc'd $C_{16}H_{26}N_7O_4ClCo$ (M+NH$_4$) = 474.1067, found 474.1064.

Co(dmgH)$_2$Cl(4-OMe-Py) isolated as orange/brown solid in 89% yield. ^{1}H NMR (500 MHz, CD_3CN): δ 7.85 (d, 2H), 6.82 (d, 2H), 3.80 (s, 3H), 2.31 (s, 12H). ^{13}C NMR (126 MHz, CD_3CN): δ 153.7, 152.3, 113.0, 57.1, 13.0. IR (film): 3479, 3005, 2945, 1656, 1616, 1375, 1267, 919, 833, 639 cm^{-1}. HRMS: Calc'd $C_{14}H_{21}N_5O_5ClCoLi$ (M+Li) = 440.0723, found 440.0712.

Co(dpgH)$_2$Cl(4-iPr-Py) isolated as tan solid in 71% yield. ^{1}H NMR (500 MHz, CD_3CN): δ 8.28 (d, 2H), 7.39-7.28 (m, 14H), 7.21-7.16 (m, 8H), [3.07 (q) &2.97 (q) Σ1H], [1.28 (d) &1.20 (d) Σ6H]. ^{13}C NMR (126 MHz, CD_3CN): δ 154.4, 151.1, 130.8, 130.6, 130.5, 129.0, 125.9, 34.0, 22.8. IR (film): 3565, 3006, 2970, 2925, 1695, 1674, 1652, 1370, 638 cm^{-1}. HRMS: Calc'd $C_{36}H_{34}N_5O_4ClCo$ (M+H) = 694.1631, found 694.1619.

Co(dpgH)$_2$Cl(Py) isolated as tan solid in 74% yield. ^{1}H NMR (500 MHz, CD_3CN): δ 8.46 (d, 2H), 7.95 (t,1H), 7.49 (t, 2H), 7.37-7.29 (m, 12H), 7.19-7.17 (m, 8H). ^{13}C NMR (126 MHz, CD_3CN): δ 154.6, 151.7, 141.1, 130.8, 130.5, 129.0, 127.6. IR (film): 3379, 3055, 2987, 1675, 1651, 1419, 896, 750, 639 cm^{-1}. HRMS: Calc'd $C_{33}H_{28}N_5O_4ClCo$ (M+H) = 652.1162, found 652.1154.

Co(dpgH)$_2$Cl(1,2-dimethylimidazole) isolated as light brown solid in 97% yield. ^{1}H NMR (500 MHz, CD_3CN): δ 7.36-7.28 (m, 12H), 7.24-7.20 (m, 8H), 7.0 (d, 1H), 6.84 (d, 1H), 3.50 (s, 3H), 2.46 (s, 3H). ^{13}C NMR (126 MHz, CD_3CN): δ 154.8, 131.7, 131.3, 131.1, 131.0, 129.4, 129.3, 127.6, 123.0, 35.5, 12.1. IR (film): 3375, 3058, 2989, 1671, 1652, 1435, 896, 749, 639 cm^{-1}. HRMS: Calc'd $C_{33}H_{31}N_6O_4ClCo$ (M+H) = 669.1427, found 669.1434.

Co(dpgH)$_2$Cl(N-Me-Imidazole) isolated as brown solid in 69% yield. ^{1}H NMR (500 MHz, CD_3CN): δ [7.71 (s) & 7.55 (s) Σ1H], 7.44-7.28 (m, 12H), 7.25-7.20 (m, 5H), 7.18-7.14 (m, 3H), [7.12 (s) & 6.88 (s) Σ1H], 7.01 (d, 1H), [3.72 (s) & 3.66 (s) Σ3H]. ^{13}C NMR (126 MHz, CD_3CN): δ 153.8, 131.1, 130.55, 130.49, 130.0, 129.0, 128.9, 128.0, 36.0. IR (film): 3522, 3006, 2970, 2925, 1657, 1417, 1370, 908, 638 cm^{-1}. HRMS: Calc'd $C_{32}H_{29}N_6O_4ClCo$ (M+H) = 655.1271, found 655.1243.

Synthesis of Co(dmgH)$_2$(butyl)Py: Modified from literature procedure.[28] A 100 mL Schlenk flask was charged with a stir bar and KOH (2.67 mmol, 0.15 g). The flask was then flame dried and cooled under argon. The flask was charged with MeOH (40 mL from Acros SureSeal) and the KOH/MeOH solution was degassed via 4 sequential freeze and thaw cycles under vacuum. Once rigorously degassed, Co(dmgH)$_2$ClPy (1 mmol, 0.404 g) was added to the reaction flask and the reaction mixture was cooled to -10 °C via a saltwater ice bath. Sodium borohydride (1.3 mmol, 0.049 g) was then added and after ~10 min the reaction mixture turned dark blue. After this color change occurred, 1-bromobutane (1 mmol, 0.107 mL) was added and after ~1 min the reaction mixture became red/orange in color. The reaction was then allowed to warm to room temperature and then stirred for 30 min at room temperature. After, acetone (1.5 mL) and water (20 mL) were added. The reaction was removed from inert atmosphere, reduced to half volume, and cooled in an ice bath. Orange precipitate formed and was collected via vacuum filtration. The isolated orange crystalline material was washed with diethyl ether and dried under vacuum to provide the desired alkyl cobaloxime, *Co(dmgH)$_2$(butyl)(Py),* in 63% yield. ^{1}H NMR (500 MHz, CD_3CN): δ [8.56 (d) & 8.45 (d) Σ2H], [7.82 (t) & 7.74 (t) Σ1H], 7.34 (t) & 7.33 (t) Σ2H], [2.15 (s) & 2.04 (s) Σ12H], 1.48-1.38 (m, 2H), 1.22-1.05 (m, 2H), 0.92-0.73 (m, 2H), 0.80 (t, 3H). ^{13}C NMR (126 MHz, CD_3CN): δ 152.7, 151.7, 150.6, 150.2, 139.7, 139.0, 33.6, 31.2, 24.6, 14.2, 12.5, 12.0. HRMS: Calc'd $C_{17}H_{29}N_5O_4Co$ (M+H) = 426.1552, found 426.1544.

Synthesis of Co(dmgH)$_2$(nonyl)(N-Me-Imidazole): The procedure detailed for the synthesis of Co(dmgH)$_2$(butyl)Py was utilized with Co(dmgH)$_2$Cl(*N*-Me-Imidazole) (0.31 mmol), KOH (0.83 mmol), $NaBH_4$ (0.40 mmol), and 1-bromononane (0.31 mmol). The Co(dmgH)$_2$(nonyl)(*N*-Me-Imidazole) product was isolated as an orange solid in 57% yield. ^{1}H NMR (500 MHz, CD_3CN): δ 7.26 (s, 1H), 6.93 (t, 1H), 6.68 (t, 1H), 3.61 (s, 3H), 2.08 (s, 12H), 1.37–1.05 (m, 14H), 0.90–0.81 (m, 5H).

General Procedure for the Synthesis of α,α-disubstituted carboxylic acids (3c,3d,3f,3g): α,α-Disubstituted carboxylic acids were synthesized from unsubstituted acids following literature procedure.[3a] A solution of diisopropylamine (8.4 mmol, 1.2 mL) in dry THF (40 mL) was made in a 100 mL flame-dried Schlenk flask with stir bar under argon. The solution was cooled to -78 °C. n-Butyllithium (8.4 mmol, 3.4 mL of 2.5 M solution in hexanes) was added to the stirring solution of diisopropylamine and allowed to stir at -78 °C under argon for 30 min. A solution of primary carboxylic acid (4 mmol) in dry THF (5 mL) was made and then added dropwise to the reaction mixture. The reaction mixture was then allowed to warm to room temperature and stir at room temperature for an additional 30 min. The reaction mixture was then cooled to -78 °C and primary alkyl bromide (5 mmol) was added. The reaction was then allowed to warm to room temperature and stir at room temperature ~14 h before being quenched by 1 M HCl (20 mL) and extracted with EtOAc (3x ~20 mL ea.). Organics were combined, dried with $MgSO_4$, and concentrated. The desired acid was purified by flash column chromatography on silica with 1:5-1:20 EtOAc:Hexanes.

2-(2-cyclohexylethyl)dodecanoic acid **(3c)**: Isolated colorless oil in 22% yield. ^{1}H NMR (500 MHz, $CDCl_3$): δ 9.90 (broad s, 1H), 2.32 (q, 1H), 1.77-1.58 (m, 7H), 1.56-1.46 (m, 2H), 1.32-1.18 (m, 22H), 0.92-0.81 (m, 5H). ^{13}C NMR (126 MHz, $CDCl_3$): δ 45.9, 37.9, 35.1, 33.5, 33.3, 32.3, 32.1, 29.8, 29.73, 29.66, 29.6, 29.5, 27.5, 26.8, 26.5, 22.8, 14.3. IR (film): 3220, 2922, 1709, 1467, 1456, 1423 cm^{-1}. HRMS: Calc'd $C_{20}H_{39}O_2$ (M+H) = 311.2950, found 311.2964.

2-(cyclohexylmethyl)dodecanoic acid **(3d)**: Isolated colorless oil in 24% yield. ^{1}H NMR (500 MHz, $CDCl_3$): δ 2.47 (broad s, 1H), 1.83-1.75 (m, 1H),

1.72-1.53 (m, 6H), 1.49-1.40 (m, 1H), 1.35-1.07 (m, 22H), 0.93-0.79 (m, 5H). ^{13}C NMR (126 MHz, $CDCl_3$): δ 40.1, 35.7, 33.7, 33.1, 33.0, 32.1, 29.8, 29.7, 29.6, 29.5, 27.5, 26.7, 26.7, 26.4, 26.3, 22.8, 22.5, 14.3, 14.2. IR (film): 3542, 2943, 1738, 1464, 1455 cm^{-1}. HRMS: Calc'd $C_{19}H_{37}O_2$ (M+H) = 297.2794, found 297.2799.

2-benzyldodecanoic acid **(3f)**: Isolated colorless oil in 24% yield. ^{1}H NMR (500 MHz, $CDCl_3$): δ 11.8 (s, 1H), 7.30-7.15 (m, 5H), 2.98 (dd, 1H), 2.76 (dd, 1H), 2.67 (q, 1H), 1.74-1.66 (m, 1H), 1.59-1.52 (m, 1H), 1.39-1.25 (m, 16H), 0.90 (t, 3H). ^{13}C NMR (126 MHz, CD_3CN): δ 181.8, 139.3, 129.0, 128.6, 126.5, 476, 38.3, 32.1, 31.9, 29.7, 29.62, 29.57, 29.6, 27.3, 22.8, 14.3. IR (film): 3617, 3003, 2944, 1730, 1656, 1635, 1464, 1456, 751 cm^{-1}. HRMS: Calc'd $C_{19}H_{31}O_2$ (M+H) = 291.2324, found 291.2324.

2-cyclopentyldodecanoic acid **(3g)**: Isolated white solid in 43% yield. ^{1}H NMR (500 MHz, CD_3CN): δ 2.20-2.11 (m, 1H), 2.04-1.91 (m, 1H), 1.90-1.69 (m, 2H), 1.68-1.46 (m, 6H), 1.37-1.09 (m, 18H), 0.87 (t, 3H). ^{13}C NMR (126 MHz, CD_3CN): δ 51.5, 42.7, 32.1, 31.6, 31.0, 30.9, 29.8, 29.6, 29.5, 27.8, 25.1, 25.1, 22.8, 14.3. IR (film): 3411, 2924, 1733, 1470, 1456, 1419 cm^{-1}. HRMS: Calc'd $C_{20}H_{39}O_2$ (M+H) = 269.2481, found 269.2484.

2-carbamoylcyclohexane-1-carboxylic acid **(3p)** was synthesized following literature procedure.[38] Ammonium hydroxide (15 mL) was added to 100 mL round-bottom flask with stir bar and cooled to 0 °C. Cyclohexane anhydride (10 g) was added portion wise and then the reaction mixture was allowed to stir overnight. The reaction was then acidified with 12 N HCl during which a precipitate formed. The precipitate was collected via vacuum filtration, washed with H_2O (~40 mL) then Et_2O (~40 mL), and dried under vacuum. ^{1}H NMR (500 MHz, d-DMSO): δ 11.89 (broad s, 1H), 7.12 (s, 1H), 6.71 (s, 1H), 2.62 (q, 1H), 2.01-1.86 (m, 2H), 1.68-1.55 (m, 2H), 1.54-1.43 (m, 1H), 1.41-1.22 (m, 3H). ^{13}C NMR (126 MHz, d-DMSO): δ 175.6, 175.2, 42.0, 41.7, 27.3, 25.7, 23.7, 23.0.

General Procedures for Co/Acr$^+$ Decarboxylative Elimination:

1) Pre-reduction Method:

A dry 10mL Schlenk flask equipped with stir bar was charged with cobaloxime (0.006 mmol, 3 mol%), sodium triacetoxyborohydride (3.2 mg, 0.015 mmol, 7.5 mol%), Na_2CO_3 (0.2 mg, 0.002 mmol, 1 mol%), and dry MeOH (0.5 mL). The reaction mixture was put under argon and fitted with a reflux condenser. The reaction mixture was stirred and refluxed at 57 °C for 50 minutes, in which time the reaction mixture went from light yellow to red. After 50 min, the flask was removed from the heat and allowed to cool for 10 min (see Supporting Information for images).

An oven-dried screw-threaded glass tube equipped with stir bar was charged with carboxylic acid (0.2 mmol, 1 equiv.) and photocatalyst (0.01 mmol, 5 mol%). A 15 mM stock solution of H_2O (1.1 µL) in MeOH (4 mL) was made and 1 mL of the stock solution was transferred to the tube. Then, dry MeOH (0.5 mL) was added and the tube was sealed with a rubber septum and screw cap. After the vial was sealed, it was sparged with argon for 5 min through the septum using a 20-gauge needle to bubble gas through the solvent, and another needle was used to vent the vial. After the flask was sparged, the sparging needle was removed from the solution but left in the vial during the addition of the cobalt catalyst solution. Another 20-gauge needle with 5 mL syringe was used to transfer the cobalt catalyst solution from the Schlenk flask to the reaction tube. After the addition of the cobalt catalyst, the sparging and venting needles were removed from the septum of the reaction tube, and the top of the tube was wrapped with parafilm. The reaction was placed in front of two 450 nm 32 W blue LED lights for 16 hours with no distance in between the reaction vessel and the light source (see Supporting Information for images). The reaction mixture was found to reach 38 °C upon irradiation in this reaction set-up. After irradiation, the final reaction mixture was condensed and purified via flash column chromatography on silica with mixtures of ethyl acetate and hexanes as the eluent. Note: enamide and enecarbamate products were found to degrade in chloroform.

2) In Situ Reduction Method

An oven-dried screw-threaded glass tube equipped with stir bar was charged with carboxylic acid (0.2 mmol, 1 equiv.), photocatalyst (0.01 mmol, 5 mol%), cobaloxime (0.006 mmol, 3 mol%), sodium triacetoxyborohydride (3.2 mg, 0.015 mmol, 7.5 mol%), and Na_2CO_3 (0.2 mg, 0.002 mmol, 1 mol%). A 15 mM stock solution of H_2O (1.1 µL) in MeOH (4 mL) was made and 1 mL of the stock solution was transferred to the tube. Then, dry MeOH (1 mL) was added and the tube was sealed with a rubber septum and screw cap. After the vial was sealed, it was sparged with argon for 5 min through the septum using a 20-gauge needle to bubble gas through the solvent, and another needle was used to vent the vial. The sparging and venting needles were removed from the septum of the reaction tube and the top of the tube was wrapped with parafilm. The reaction was placed in front of two 450 nm 32 W blue LED lights for 16 hours with no distance in between the reaction vessel and the light source (see Supporting Information for images). Irradiation and purification process the same as described in pre-reduction procedure.

Enamide and enecarbamate products **2a-2v** were previously synthesized in our lab (also see Table S1).[3c]

(E)-1-phenylbut-2-en-1-one **(4a)**: Isolated amorphous white solid. ^{1}H NMR (500 MHz, $CDCl_3$): δ 7.96–7.87 (m, 2H), 7.59–7.50 (m, 1H), 7.47 (dd, 2H), 7.08 (dq, 1H), 6.94–6.87 (m, 1H), 2.00 (dd, 3H). ^{13}C NMR (126 MHz, CD_3CN): δ 190.7, 144.9, 137.8, 132.5, 128.4, 127.4, 18.5. IR (film): 3072, 2923, 1718, 1652, 1605, 1454, 935, 750 cm^{-1}. HRMS: Calc'd $C_{10}OH_{14}N$ (M+NH_4) = 164.1075, found 164.1077.

(E)-pentadec-6-ene & (E)-pentadec-7-ene **(4b)**: Isolated mix of regioisomers as colorless oil. ^{1}H NMR (500 MHz, $CDCl_3$): δ [5.44-5.37 (m) & 5.37-5.31 (m) Σ2H], [2.06-2.00 (m) & 2.00-1.93 (m), Σ4H], 1.4-1.18 (m, 18H), 0.89 (t, Σ6H). ^{13}C NMR (126 MHz, $CDCl_3$): δ 130.5, 130.0, 32.8, 32.7, 32.08, 32.05, 31.9, 31.6, 30.0, 29.84, 29.80, 29.7, 29.52, 29.49, 29.37, 29.35, 29.3, 29.0, 27.4, 27.3, 22.9, 22.8, 22.7, 14.3. IR (film): 3005, 2956, 1636, 1466, 1455, 966, 723 cm^{-1}. See Supporting Information for GC/MS data and COSY spectra.

(E)-tridec-2-en-1-ylcyclohexane & (E)-tridec-3-en-1-ylcyclohexane **(4c)**: Isolated mix of regioisomers as a colorless oil. ^{1}H NMR (500 MHz, $CDCl_3$): (1.95:1 regioisomer ratio) δ 5.46-5.33 (m, 2H), 2.10-1.97 (m, 3H), 1.97-1.84 (m, 1H), 1.77-1.61 (m, 5H),1.41-1.11 (m, 20H), 0.97-0.81 (m, 5H). ^{13}C NMR (126 MHz, $CDCl_3$): δ 131.6, 130.7, 130.3, 128.9, 20.8, 38.3, 37.6, 37.3, 33.5, 32.81, 32.79, 32.1, 29.9, 29.8, 29.71, 29.69, 29.53, 29.52, 29.4, 29.3, 26.9, 26.8, 26.58, 26.56, 22.9, 12.4. IR (film): 3004, 2925, 1466, 1449, 967, 721 cm^{-1}. See Supporting Information for GCMS data and COSY spectra.

(E)-dodec-1-en-1-ylcyclohexane & (E)-dodec-2-en-1-ylcyclohexane **(4d)**: Isolated mix of regioisomers (3.6:1 A:B) and geometric isomers (>95:5 E:Z) as a colorless oil. ^{1}H NMR (500 MHz, $CDCl_3$): (3.6:1 isomer ratio) δ [5.43-5.30 (m) & 5.28-5.15 (m) Σ2H], 2.34-1.20 (m, 0.4H, only minor isomer), 2.06-1.83 (m, Σ4H), 1.75-1.58 (m, Σ5H), 1.39-0.98 (m, Σ22H), 0.94-0.75 (m, Σ6H). ^{13}C NMR (126 MHz, $CDCl_3$): δ 136.5, 131.6, 128.9, 127.9, 40.9, 38.3, 33.5, 33.3, 32.8, 32.1, 29.9, 29.81, 29.78, 29.7, 29.5, 29.34, 29.31, 26.8, 26.6, 26.4, 26.3, 22.9, 14.3. IR (film): 3055, 2927, 1652, 1634, 1464, 1450, 971, 720 cm^{-1}. See Supporting Information for GC/MS data and COSY spectra.

(E)-2,2,4,8,10,10-hexamethylundec-5-ene & (E)-2,2,4,8,10,10-hexamethylundec-4-ene **(4e)**: Isolated mix of geometric and regioisomers as a colorless oil. ^{1}H NMR (500 MHz, $CDCl_3$): (86:14 geometric isomer ratio, >90:10 regioisomer ratio) δ [5.43-5.10 (m) Σ2H], [2.58-2.51 (m) 0.15H, only minor isomer)], [2.28-2.19 (m) 0.84H, only major isomer], [2.11-1.98 (m) 0.19H only minor isomer], [1.96-1.88 (m) Σ1H], [1.86-1.78 (m) 0.85H, only major isomer], [1.58-1.39 (m) Σ1H], [1.32-1.13 (m) Σ4H], [1.07-0.79 (m) Σ26H]. ^{13}C NMR (126 MHz, $CDCl_3$): δ 140.11, 140.08, 126.4, 126.3, 51.4, 50.6, 50.5, 42.7, 34.1, 30.4, 30.3, 30.2, 29.90, 29.86, 24.43, 24.41, 22.8, 22.7. IR (film): 3053, 2954, 1645, 1464, 1449, 968, 638 cm^{-1}. See Supporting Information for GCMS data and COSY spectra.

(E)-dodec-1-en-1-ylbenzene & (E)-dodec-2-en-1-ylbenzene **(4f)**: Isolated mix of geometric and regioisomers as well as alkane product as a colorless oil. ^{1}H NMR (500 MHz, $CDCl_3$): (3:1 E:Z, >95:5 regioisomer ratio, 2:1 alkene:alkane) δ 7.32-7.27 (m, 2H), 7.23-7.16 (m, 3H), 5.61-5.46 (m, 2H), [3.41 (d) & 3.34 (d) Σ2H], [2.61 (t) & 2.15 (t) Σ1H], 2.03 (td, 2H), 1.66-1.58 (m, 1H), 1.43-1.21 (m, 20H), 0.89 (t, 4H). ^{13}C NMR (126 MHz, $CDCl_3$): δ

143.1, 141.3, 132.3, 131.2, 128.8, 128.6, 128.54, 128.49, 128.46, 128.1, 125.98, 125.94, 125.7, 39.2, 36.2, 33.7, 32.7, 32.1, 31.7, 29.83, 29.76, 29.7, 29.5, 29.4, 27.4, 22.8, 14.3. IR (film): 3063, 2956, 1699, 1652, 1604, 1464, 1454, 968, 744 cm^{-1}. See Supporting Information for GC/MS data and COSY spectra.

(E)-undec-1-en-1-ylcyclopentane & undecylidenecyclopentane **(4g)**: Isolated mix of geometric and regioisomers as a colorless oil. ^{1}H NMR (500 MHz, $CDCl_3$): (80:20 E:Z, >95:5 regioisomer ratio) δ [5.43-5.31 (m) & 5.30-5.23 (m) Σ2H], [2.73-2.63 (m) & 2.41-2.33 (m) Σ1H], [2.08-2.00 (m) & 1.99-1.92 (m) Σ2H], 1.79-1.70 (m, 2H), 1.69-1.46 (m, 5H), 1.37-1.18 (m, 19H), 0.93-0.83 (m, 4H). ^{13}C NMR (126 MHz, $CDCl_3$): δ 135.7, 135.4, 128.8, 43.8, 40.6, 38.6, 36.7, 34.2, 33.7, 33.0, 32.3, 30.4, 30.14, 30.12, 30.02, 29.98, 29.8, 29.7, 29.6, 29.2, 27.9, 25.8, 25.6, 25.5, 23.1, 14.5. IR (film): 3054, 2925, 1660, 1467, 1456, 970, 705 cm^{-1}. See Supporting Information for GC/MS data and COSY spectra.

4'-ethyl-[1,1'-bi(cyclohexan)]-3-ene **(4h)**: Isolated as colorless oil. ^{1}H NMR (500 MHz, $CDCl_3$): δ 5.66 (m, 2H), 2.11-1.95 (m, 3H), 1.83-1.67 (m, 6H), 1.39-1.29 (m, 1H), 1.27-1.14 (m, 3H), 1.12-1.02 (m, 2H), 1.04-0.91 (m, 2H), 0.87 (m, 5H). ^{13}C NMR (126 MHz, $CDCl_3$): δ 127.3, 127.2, 43.0, 39.9, 39.4, 33.3, 30.2, 30.0, 29.3, 26.4, 26.2. IR (film): 3022, 2960, 1668, 1447, 896, 705 cm^{-1}. See Supporting Information for GCMS data and COSY spectra.

tert-butyl (cyclohex-3-en-1-ylmethyl)carbamate **(4i)**: Isolated as colorless oil. ^{1}H NMR (500 MHz, $CDCl_3$): δ 5.69-5.60 (m, 2H), 4.61 (broad s, 1H), 3.09-3.00 (m, 2H), 2.13-1.99 (m, 3H), 1.78-1.64 (m, 3H), 1.44 (s, 9H). ^{13}C NMR (126 MHz, $CDCl_3$): δ 127.5, 126.1, 46.4, 34.7, 29.6, 28.8, 26.7, 25.1. HRMS: Calc'd $C_{12}H_{22}O_2NNa$ (M+Na) = 235.1548, found = 235.1560. IR (film): 3343, 2915, 1689, 1519, 1365, 1206, 1150 cm^{-1}.

cyclohex-3-en-1-ol **(4j)**: Isolated as colorless oil. ^{1}H NMR (500 MHz, $CDCl_3$): δ 5.70-5.62 (m, 1H), 5.61-5.51 (m, 1H), 3.99-3.91 (m, 1H), 2.42-2.30 (m, 1H), 2.23-2.06 (m, 2H), 2.05-1.95 (m, 1H), 1.91-1.81 (m, 1H), 1.08-1.54 (m, 2H). ^{13}C NMR (126 MHz, $CDCl_3$): δ 126.9, 124.2, 67.1, 34.5, 31.0, 23.7. IR (film): 3465, 3054, 2987, 1652, 1464, 1421, 1150, 705 cm^{-1}. HRMS: Calc'd $C_6H_{14}ON$ (M+NH_4) = 116.1075, found = 116.1070.

cyclohex-3-en-1-yl acetate **(4k)**: Isolated as colorless oil. ^{1}H NMR (500 MHz, $CDCl_3$): δ 5.71-5.65 (m, 1H), 5.59-5.55 (m, 1H), 5.04-4.97 (m, 1H), 2.43-2.33 (m, 1H), 2.21-2.1 (m, 3H), 1.93-1.84 (m, 1H), 1.76-1.67 (m, 1H). ^{13}C NMR (126 MHz, $CDCl_3$): δ 170.9, 126.9, 123.8, 69.9, 30.9, 27.4, 23.4, 21.6. IR (film): 3058, 2990, 1698, 1644, 1422, 1211, 1152, 896, 749 cm^{-1}. HRMS: Calc'd $C_8H_{12}O_2Na$ (M+Na) = 163.0735, found = 163.0740.

4'-chloro-1,2,3,6-tetrahydro-1,1'-biphenyl **(4l)**: Isolated as colorless oil. ^{1}H NMR (500 MHz, $CDCl_3$): δ 7.29 (d, 2H), 7.18 (d, 2H), 5.80-5.76 (m, 2H), 2.85-2.77 (m, 1H), 2.34-2.24 (m, 1H), 2.23-2.08 (m, 3H), 1.96-1.89 (m, 1H), 1.79-1.69 (m, 1H). ^{13}C NMR (126 MHz, $CDCl_3$): δ 145.6, 131.4, 128.3, 128.1, 126.9, 126.4, 39.4, 22.2, 29.5, 25.6. IR (film): 3024, 2914, 1665, 1652, 1464, 824, 668, 643 cm^{-1}. HRMS: Calc'd $C_{10}ClH_{13}$ (M+H) = 168.0706, found = 168.0705.

tert-butyl cyclohex-2-en-1-ylcarbamate & tert-butyl cyclohex-3-en-1-ylcarbamate **(4m)**: Isolated a mix of regioisomers (63:36) as colorless oil. ^{1}H NMR (500 MHz, $CDCl_3$): δ [5.81-5.76 (m) & 5.67-5.62 (m) & 5.59-5.55 (m), Σ2H], [4.5 (broad s) & 3.77 (broad s), Σ1H], 2.41-2.32 (m, 1H), 2.17-2.07 (m, 1H), 2.01-1.93 (m, 1H), 1.92-1.79 (m, 2H), 1.69-1.58 (m, 1H), 1.58-1.47 (m, 1H), 1.44 (s, 9H). ^{13}C NMR (126 MHz, $CDCl_3$): δ 171.3, 155.5, 130.5, 128.3, 127.1, 124.6, 80.0, 60.5, 45.8, 33.7, 32.2, 29.9, 28.6, 25.7, 24.9, 23.8, 21.2, 19.8, 14.3. IR (film): 3353, 3025, 2978, 1682, 1652, 1464, 1180, 668 cm^{-1}. HRMS: Calc'd $C_{11}H_{19}NO_2Na$ (M+Na) = 220.1313, found 220.1314.

benzyl cyclohex-1-en-1-ylcarbamate & benzyl cyclohex-2-en-1-ylcarbamate **(4n)**: Isolated a mix of regioisomers (95:5) as an amorphous white solid. ^{1}H NMR (500 MHz, CD_3CN): δ 7.47-7.27 (m, 5H), 5.82 (m, 1H), [5.64 (broad s) & 5.53 (broad s) Σ1H], 5.05 (m, 2H), 4.11 (m, 1H), 2.18 (s, 1H), 2.03-1.96 (m, 1H), 1.89-1.82 (m, 1H), 1.74-1.65 (m, 1H), 1.64-1.55 (m, 1H), 1.55-1.46 (m, 1H), [1.36-1.26 (m) & 1.22-1.11 (m) Σ1H]. ^{13}C NMR (126 MHz, CD_3CN): δ 156.7, 138.5, 130.9, 129.4, 129.1, 128.8, 128.7, 66.7, 47.5, 30.4, 25.4, 20.6. IR (film): 3521, 3061, 3001, 2942, 1716, 1644, 1634, 1463, 1272, 1165, 918, 897, 749, 638 cm^{-1}. HRMS: Calc'd $C_{14}H_{18}NO_2$ (M+H) = 232.1338, found 232.1346.

methyl cyclohex-1-ene-1-carboxylate & methyl cyclohex-2-ene-1-carboxylate **(4o)**: Isolated a mix of regioisomers (63:37) as a colorless oil. ^{1}H NMR (500 MHz, $CDCl_3$): δ [6.99-6.96 (m), 5.87-5.82 (m), 5.77-5.72 (m), Σ2H], [3.72 (s), 3.69 (s), 3.65 (s), Σ3H], 3.13-3.07 (m, 1H), [2.28-2.22 (m), 2.2-2.15 (m), Σ2H], 2.08-1.95 (m, 1H), 1.95-1.71 (m, 2H), 1.69-1.54 (m, 2H). ^{13}C NMR (126 MHz, $CDCl_3$): δ 175.2, 168.2, 139.9, 129.8, 124.4, 51.9, 51.6, 41.2, 29.2, 25.9, 25.4, 24.8, 24.3, 22.2, 21.6, 20.9. IR (film): 3003, 2944, 1634, 1441, 1224, 1153, 919, 750, 640 cm^{-1}. HRMS: Calc'd $C_8H_{13}O_2$ (M+H) = 141.0916, found 141.0921.

cyclohex-1-ene-1-carboxamide & cyclohex-2-ene-1-carboxamide **(4p)**: Isolated mix of regioisomers (80:20) as an amorphous white solid. ^{1}H NMR (500 MHz, $CDCl_3$): δ [6.71-6.67 (m), 5.94 (dq), 5.72 (dq), Σ3H], 3.00-2.93 (m, 1H), [2.25-2.20 (m), 2.19-2.14 (m), Σ1H], 2.12-1.97 (m, 1H), 1.96-1.82 (m, 2H), 1.78-1.55 (m, 2H). ^{13}C NMR (126 MHz, $CDCl_3$): δ 177.7, 170.8, 135.3, 132.4, 131.6, 124.6, 42.7, 26.6, 25.6, 25.0, 24.4, 22.2, 21.5, 20.5. HRMS: Calc'd $C_7H_{12}NO$ (M+H) = 126.0919, found = 126.0912. IR (film): 3345, 3182, 2930, 2833, 1662, 1627, 1412, 1208, 1152, 898, 624 cm^{-1}.

5. Acknowledgements

This work was supported by the National Science Foundation (CHE-1800147) and the Kansas Bioscience Authority Rising Star program. Support for the NMR instrumentation was provided by NSF Academic Research Infrastructure Grant No. 9512331, NIH Shared Instrumentation Grant No. S10RR024664, and NSF Major Research Instrumentation Grant No. 0320648.

Keywords: dual catalysis • photoredox • cobaloxime • decarboxylative • hydrogen evolution

6. References

[1] Reviews: a) H. Huang, K. Jia, Y. Chen, *ACS Catal.* **2016**, *6*, 4983-4988. b) J. Xuan, Z.-G. Zhang, W.-J. Xiao, *Angew. Chem., Int. Ed.* **2015**, *54*, 15632−15641. c) R. A. Angnes, Z. Li, C. R. D. Correia, G. B. Hammond, *Org. Biomol. Chem.* **2015**, *13*, 9152−9167. Select examples: d) A. Tlahuext-Aca, L. Candish, R. A. Garza-Sanchez, F. Glorius, *ACS Catal.* **2018**, *8*, 1715−1719. e) K. Xu, Z. Tan, H. Zhang, J. Liu, S. Zhang, Z. Wang, *Chem. Commun.* **2017**, *53*, 10719-10722. f) S. B. Lang, K. C. Cartwright, R. S. Welter, T. M. Locascio, J. A. Tunge, *Eur. J. Org. Chem.* **2016**, 3331−3334. g) Z. Zuo, D. T. Ahneman, L. Chu, J. A. Terrett, A. G. Doyle, D. W. C. MacMillian, *Science*, **2014**, *345*, 436-440. h) S. Ventre, F. R. Petronijevic, D. W. MacMillan, *J. Am. Chem. Soc.* **2015**, *137*, 5654−5657. i) S. B. Lang, K. M. O'Nele, J. A. Tunge, *J. Am. Chem. Soc.* **2014**, *136*, 13606−13609. j) Z. Zuo, D. W. C. MacMillan, *J. Am. Chem. Soc.* **2014**, *136*, 5257−5260. k) Y. Miyake, K. Nakajima, Y. Nishibayashi, *Chem. Commun.* **2013**, *49*, 7854−7856.

[2] Decarbonylative strategies towards olefins: (a) P. García-Reynaga, A. K. Carrillo, M. S. VanNieuwenhze *Org. Lett.* **2012**, *14*, 1030−1033. Decarboxylative strategies for olefination: (b) A. B. Miller, Nelson, J. A. M. P. Byrne, *J. Org. Chem.* **1993**, *58*, 18−20. (c) L. J. Gooßen, Rodriguez *N. Chem. Commun.* **2004**, *0*, 724−725. (d) S. Maetani, T. Fukuyama, N. Suzuki, D. Ishihara, I. Ryu, *Organometallics* **2011**, *30*, 1389−1394. (e) S. Maetani, T. Fukuyama, N. Suzuki, D. Ishihara, I. Ryu, *Chem. Commun.* **2012**, *48*, 2552− 2554. (f) M. O. Miranda, A. Pietrangelo, M. A. Hillmyer, W. B. Tolman *Green Chem.* **2012**, *14*, 490−494. (g) R. E. Murray, E. L. Walter, K. M. Doll, *ACS Catal.* **2014**, *4*, 3517−3520. (h) Y. Liu, K. E. Kim, M. B. Herbert, A. Fedorov, R. H. Grubbs, B. M. Stoltz, *Adv. Synth. Catal.*

2014, *356*, 130−136. (i) A. John, M. O. Miranda, K. Ding, B. Dereli, M. A. Ortuño, A. M. LaPointe, G. W. Coates, C. J. Cramer, W. B. Tolman, *Organometallics* **2016**, *35*, 2391−2400. (j) A. John, M. A. Hillmyer, W. B. Tolman *Organometallics* **2017**, *36*, 506−509. (k) A. Chatterjee, S. H. Eliasson, K. W. Törnroos, V. R. Jensen *ACS Catal*. **2016**, *6*, 7784−7789. (l) A. Tlahuext-Aca, L. Candish, R. A. Garza-Sanchez, F. Glorius *Chem. Eur. J*. **2018**, *24*, 4552-4555.

[3] Photoredox dual catalysis decarboxylative elimination methods: a) A. Tlahuext-Aca, L. Candish, R. A. Garza-Sanchez, F. Glorius, *ACS Catal.* **2018**, *8*, 1715−1719. b) X. Sun, J. Chen, T. Ritter, *Nat. Chemistry* **2018**, *10*, 1229-1233. c) K. C. Cartwright, J. A. Tunge, *ACS Catal.* **2018**, *8*, 11801-11806. d) V. T. Nguyen, V. D. Nguyen, G. C. Haug, H. T. Dang, S. Jin, Z. Li, C. Flores-Hansen, B. S. Benavides, H. D. Arman, O.V. Larionov, *ACS Catal.* **2019**, *9*, *10*, 9485-9498. e) H. Cao, H. Jiang, J. M. C. Kwan, X. Liu, J. Wu, *J. Am. Chem. Soc.* **2018**, *140*, 16360-16367.

[4] a) R. A. Sheldon, J. K. Kochi, *Org. React.* **1972**, *19*, 279.; b) Kochi, J. K.; Bemis, A.; Jenkins, C. L. *J. Am. Chem. Soc*. **1968**, *90*, 4616−4625. c) J. K. Kochi, *Science,* **1967**, *155*, 415−424.

[5] a) S-W. Wu, J-L. Lui, F. Liu, *Org. Lett.* **2016**, *18*, 1-3. b) K. C. Cartwright, S. B. Lang, J. A. Tunge, *J. Org. Chem.* **2019**, *84*, 2933.

[6] J. Cornella, J. T. Edwards, T. Qin, S. Kawamura, J. Wang, C-M. Pan, R. Gianatassio, M Schmidt, M. D. Eastgate, P. S. Baran, *J. Am. Chem. Soc.*, **2016**, *138*, 2174-2177.

[7] Redox active ester synthesis generally utilizes *N*-hydroxyphthalimide (100g = $36.00 from Sigma) and DCC (100g = 55.60 from Sigma). The use of redox-active esters detracts from step and atom economy. Ideal synthesis reviews: a) T. Newhouse, P. S. Baran, R. W. Hoffmann, *Chem. Soc. Rev*. **2009**, *38*, 3010. b) T. Gaich, P. S. Baran, *J. Org. Chem*. **2010**, *75*, 4657.

[8] Reviews that disscuss PC/Co H_2 evolution in cross-couplings: a) K. C. Cartwright, A. M. Davies, J. A. Tunge *Eur. J. Org. Chem*. **2019**. DOI: 10.1002/ejoc.201901910. b) S. Tang, L. Zeng, A. Lei, *J. Am. Chem. Soc.* **2018**, *140*, 13128-13135. c) B. Chen, L.-Z. Wu, C.-H. Tung, *Acc. Chem. Res.* **2018**, *51*, 2512-2523. Review on HAT in photocatalyzed organic synthesis: d) L. Capaldo, D. Ravelli, *Eur. J. Org. Chem.* **2017**, 2056-2071.

[9] Potentials in Figure 1 are reported vs. SCE in MeCN. Acridinium catalysts: a) S. Fukuzumi, H. Kotani, K. Ohkubo, S. Ogo, N. V. Tkachenko, H. Lemmetyinen, *J. Am. Chem. Soc.* **2004**, *126*, 1600. Recent protocol for acridinium salt synthesis: b) A. R. White, L. Wang, D. A. Nicewicz, *Synlett* **2019**, *30*, A–F. Potentials reported for the acridinium photocatalyst: c) N. A. Romero, K. A. Margrey, N. E. Tay, D. A. Nicewicz, *Science* **2015**, *349*, 1326−1330. d) D. S. Hamilton, D. A. Nicewicz, *J. Am. Chem. Soc*. **2012**, *134*, 18577–18580. e) A. Joshi-Pangu, F. Lévesque, H. G. Roth, S. F. Oliver, L.-C. Campeau, D. Nicewicz, D. A. DiRocco, *J. Org. Chem.* **2016**, *81*, 7244-7249. For a review on organic photoredox catalysis: f) N. A. Romero, D. A. Nicewicz, *Chem. Rev*. **2016**, *116*, 10075-10166. Potentials of carboxylates: g) J. D. Griffin, M. A. Zeller, D. A. Nicewicz, *J. Am. Chem. Soc*., **2015**, *137*, 11340-11348. Counter ion influence: h) T. G. Beaumont, K. M. C. Davis, *J. Chem. Soc. B*, **1970**, 456–459.

[10] a) G. Dutta, M. Laskar, B. D. Gupta, *Organometallics* **2008**, *27*, 3338–3345. b) M. Bhuyan, M. Laskar, D. Mandal, B. D. Gupta, *Organometallics* **2007**, *26*, 3559-3567. c) B. D. Gupta, R. Yamuna, D. Mandal, *Organometallics* **2006**, *25*, 706-714. c) D. Mandal, B. D. Gupta, *Organometallics,* **2005**, *24*, 1501-1510. d) B. D. Gupta, V. Singh, R. Yamuna, T. Barclay, W. Cordes, *Organometallics* **2003**, *22*, 2670-2678. e) B. P. Branchaud, Y. L. Choi, *Tet. Lett.* **1988**, *29*, 6037-6038.

[11] a) David R. Lide, ed., *CRC Handbook of Chemistry and Physics, Internet Version,* <http://www.hbcpnetbase.com>, CRC Press, Boca Raton, FL, **2005**. b) R. J. L. Andon, J. D. Cox, E. F. G. Herington, *Trans. Faraday Soc.*, **1954**, *50,* 918. c) E. Chrystiuk, A. Williams, *J. Am. Chem. Soc.,* **1987**, *109*, 3040. d) J. A. Dean, N. A. Lange, *Lange's Handbook of Chemistry*; McGraw-Hill, **1934**. e) J. Buckingham, *Dictionary of Organic Compounds*; Chapman & Hall, **1996**. f) S. Hensel, N. Megger, K. Schweizer, J. Müller, *Beilstein J. Org. Chem.* **2014,** *10,* 2139–2144. g) T. Allman, R. G. Goel *Can. J. Chem.,* **1982**, *60,* 716.

[12] a) A. Panagiotopoulos, K. Ladomenou, D. Sun, V. Artero, A. G. Coutsolelos, *Dalton Trans*., **2016**, *45*, 6732-6738. b) M. A. W. Lawrence, M. J. Celestine, E. T. Artis, L. S. Joseph, D. L. Esquivel, A. J. Ledbetter, D. M. Cropek, W. L. Jarrett, C. A. Bayse, M. L. Brewer, A. A. Holder, *Dal. Trans,* **2016**, *45*, 10326-10342. c) S. Mirra, M. Strianese, C. Pellecchia, V. Bertolasi, G. Monaco, S. Milione, *Inorganica Chimica Acta*, **2016**, *444*, 202-208. d) Y. Noboru, H. Yorikatsu, *Bulletin of the Chemical Society of Japan,* **1971,** *44*, 63-69**.** e) A. Kilic, M. Durgun, N. Yorulmaz, R. Yavuz, *J. Molecular Structure,* **2018**, *1174,* 25-31. f) R. C. Stewart, L. G. Marzilli, *J. Am. Chem. Soc.* **1977**, *111,* 817-822.

[13] D. E. Moore, *International Journal of Pharmaceutics*, **1990**, *63*, R5-R7.

[14] J. K. Kochi *Pure & Appl. Chem*., **1991**, *63*, 2, 255-264.

[15] K. D. Collins, F. Glorius, *Nat. Chem.* **2013**, *5*, 597-601.

[16] a) G. Li, A. Han, D. P. Estes, J. R. Norton, *J. Am. Chem. Soc.* **2012**, *134*, 14662-14665. b) D. P. Estes, D. C. Grills, J. R. Norton, *J. Am. Chem. Soc*. **2014**, *136*, 17362−17365.

[17] a) B. Giese, *Radicals in Organic Synthesis: Formation of Carbon–Carbon Bonds*, Pergamon Press, Oxford, 1986. b) Acr-promoted Giese-type reaction with carboxylic acids: N. P. Ramierz, J. C. Gonzalez-Gomez, *Eur. J. Org. Chem.* **2016**, *2017*, 2154-2163.

[18] Potentially the catalyst interuption involves that formation of a Acr^+/carboxylate complex similar to that discribed in Section 2.1.3 and Figure S5 and S6.

[19] A. F. Abdel-Magid, S. J. Mehrman, *Organic Process Research & Development* **2006**, *10*, 971-1031.

[20] a) T. Lazarides, T. McCormick, P. Du, G. Luo, B. Lindley, R. Eisenberg, *J. Am. Chem. Soc.* **2009**, *131*, 9192-9194. Additional reports of additional dmgH improving HE: b) W. T. Eckenhoff, W. R. McNamara, P. Du, R. Eisenberg, *Biochim. Biophys. Acta, Bioenerg*. **2013**, *1827*, 958−973. c) T. M. McCormick, Z. Han, D. J. Weinberg, W. W. Brennessel, P. L. Holland, R. Eisenberg, *Inorg. Chem.* **2011**, *50*, 10660−10666. d) T. Banerjee, F. Haase, G. Savasci, K. Gottschling, C. Ochenfeld, B. V. Lotsch, *J. Am. Chem. Soc.* **2017**, *139*, 16228−16234.

[21] a) S. Senaweera, K. C. Cartwright, J. A. Tunge, *J. Org. Chem.* **2019**, *84*, 12553-12561. b) B. J. Lee, K. S. DeGlopper, T. P. Yoon, *Angew. Chem. Int. Ed.* **2020**, *59*, 197-202.

[22] S. W. Benson, *J. Phys. Chem*. **1985**, *89*, 20, 4366-4369.

[23] a) S. Takeuchi, Y. Ohgo, J. Yoshimura, *Bull. Chem. Soc. Japan* **1974**, *47*, 463-466. b) B. R. James, Hydrogenation reactions catalyzed by transition metal complexes, in F.G.A. Stone, W. Roberts (Eds.), Adv. Organomet. Chem., Academic Press, **1979**, pp. 319-405.

[24] When substrate **3b** was irradiated for 72 hours, a 60:40 ratio of alkene:alkane was observed by GC/MS.

[25] a) M. Razavet, V. Artero, M. Fontecave, *Inorg. Chem.* **2005**, *44*, 4786-4795. b) J. L. Dempsey, B. S. Brunswig, J. R. Winkler, H. B. Gray. *Acc. Chem. Res*. **2009**, *42*, 1995-2004.

[26] a) C. Creutz, M. H. Chou, E. Fujita, *Coord. Chem. Rev.* **2005**, *249*, 375-390. b) G. N. Schrauzer, E. Deutsch, *J. Am. Chem. Soc.* **1969**, *91*, 3341-3350.

[27] D. Dodd, M. D. Johnson, B. L. Lockman, *J. Am. Chem. Soc.* **1977**, *99*, 3664-3672.

[28] a) D. L. Jameson, J. J. Grzybowski, D. E. Hammels, R. K. Castellano, E. Hoke, K. Freed, S. Basquill, A. Mendel, W. J. Shoemaker. *J. Chem. Ed.* **1998**, *75*, 447-450. b) W. C. Trogler, R. C. Stewart, L. A. Epps, L. G. Marzilli, *Inorg. Chem*. **1974**, *13*, 1564–1570. c) J. Bulkowski, A. Cutler, D. Dolphin, R. B. Silverman, *Inorg. Synth*. **1980**, *20*, 127–134.

[29] X. Hu, B. S. Brunschwig, J. C. Peters, *J. Am. Chem. Soc.* **2007**, *129*, 8988-8998.

[30] Reactivity of Co-alkyls under photochemical conditions: a) B. P. Branchaud, M. S. Meier, Y. Choi, *Tet. Lett*. **1988,** *29*, 167-170. b) B. P. Branchaud, W. D. Detlefsen, *Tet. Lett.* **1991**, *32*, 6273-6276. c) B. P. Vranchaud, Y. L. Choi, *J. Org. Chem.* **1988**, *53*, 4641-4643.

[31] Rate estimate based on nonyl radical and TEMPO coupling rate in acetonitrile: A. L. J. Beckwith, V. W. Bowry, K. U. Ingold, *J. Am. Chem. Soc.* 1992, **114**, 4983-4992.

[32] The possibility of a Co-Carboxylate complex leading to the Co catalyst being in close proximinty to the alkyl radical formed should be considered: S. S. Lande, J. K. Kochi, *J. Am. Chem. Soc.* **1968**, 5196-5207.

[33] Select examples of proposed alkyl radical oxidation by Co(II): a) H. Yi, L. Niu, C. Song, Y. Li, B. Dou, A. K. Singh, A. Lei, *Angew. Chem. Int. Ed.* **2017**, *56*, 1120–1124. b) W. Cao, C. Wu, T. Lei, X. Yang, B. Chen, C. Tung, L. Wu, *Chin. J. Catal.* **2018**, *39*, 1194–1201.

[34] D. D. M. Wayner, D. J. McPhee, D. Griller, *J. Am. Chem. Soc.* **1988**, *110*, 132-137.

[35] J. T. Muckerman, E. Fujita, *Chem. Commun.* **2011**, *47*, 12456-12457.

[36] a) V. Artero, M. Chavarot-Kerlidou, M. Fontecave, *Angew. Chem. Int. Ed.* **2011**, *50*, 7238 – 7266. b) N. Fajrina, M. Tahir, *International Journal of Hydrogen Production* **2019**, *44*, 540-577.

[37] a) T. M. McCormick, B. D. Calitree, A. Orchard, N. D. Kraut, F. V. Bright, M. R. Detty, R. Eisenberg, *J. Am. Chem. Soc.* **2010**, *132*, 15480–15483. b) J. L. Dempsey, J. R. Winkler, H. B. Gray, *J. Am. Chem. Soc.* **2010**, *132*, 16774–16776. c) B. H. Solis and S. Hammes-Schiffer, *Inorg. Chem.* **2011**, *50*, 11252–11262. d) E. S. Wiedner, R. M. Bullock, *J. Am. Chem. Soc.* **2016**, *138*, 8309−8318.

[38] B. Portevin, C. Tordjman, P. Pastoureau, J. Bonnet, G. De Nanteuil, *J. Med. Chem.* **2000**, *43*, 4582-4593.

Entry for the Table of Contents

Layout 2:

FULL PAPER

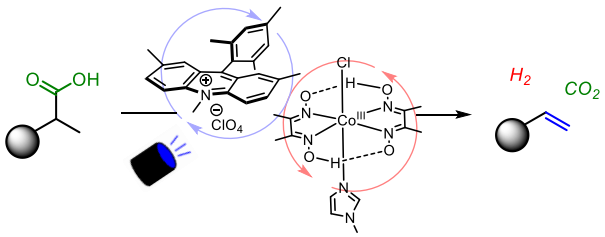

*Kaitie C. Cartwright, Ebbin Joseph, Chelsea G. Comadoll, Jon A. Tunge**

Page No. – Page No.
Photoredox/Cobalt Dual Catalyzed Decarboxylative Elimination of Carboxylic Acids: Development and Mechanistic Insight

Unveiling the power of cobaloximes in light-promoted small molecule functionalization is on the rise. The marriage of decarboxylation and hydrogen evolution in the synthesis of alkenes from carboxylic acids has been of recent interest. Herein, further developments and mechanistic insights on this elegant process are described.